



## Recent advances in synthesis, physical properties and applications of conducting polymer nanotubes and nanofibers

Yun-Ze Long<sup>a,f,\*</sup>, Meng-Meng Li<sup>a,1</sup>, Changzhi Gu<sup>b,2</sup>, Meixiang Wan<sup>c,3</sup>, Jean-Luc Duvail<sup>d,4</sup>, Zongwen Liu<sup>e,5</sup>, Zhiyong Fan<sup>f,6</sup>

<sup>a</sup> College of Physics Science, Qingdao University, Qingdao 266071, China

<sup>b</sup> Institute of Physics, Chinese Academy of Sciences, Beijing 100190, China

<sup>c</sup> Institute of Chemistry, Chinese Academy of Sciences, Beijing 100190, China

<sup>d</sup> Institut des Matériaux Jean Rouxel, CNRS, Université de Nantes, F-44322 Nantes, France

<sup>e</sup> Australian Centre for Microscopy and Microanalysis, The University of Sydney, Sydney, NSW 2006, Australia

<sup>f</sup> Department of Electronic and Computer Engineering, The Hong Kong University of Science and Technology, Kowloon, Hong Kong, China

### ARTICLE INFO

#### Article history:

Received 8 June 2010

Received in revised form 7 January 2011

Accepted 14 April 2011

Available online 17 April 2011

#### PACS:

82.35

82.35

81.05

81.07

81.16

#### Keywords:

Polyaniline

Polypyrrole

Poly(3,4-ethylenedioxythiophene)

Nanotube

Nanowire

Nanofiber

Conductivity

Sensor

Transistor

### ABSTRACT

This article summarizes and reviews the various preparation methods, physical properties, and potential applications of one-dimensional nanostructures of conjugated polyaniline (PANI), polypyrrole (PPY) and poly(3,4-ethylenedioxythiophene) (PEDOT). The synthesis approaches include hard physical template method, soft chemical template method, electrospinning, and lithography techniques. Particularly, the electronic transport (e.g., electrical conductivity, current–voltage ( $I$ – $V$ ) characteristics, magnetoresistance, and nanocontact resistance) and mechanical properties of individual nanowires/tubes, and specific heat capacity, magnetic susceptibility, and optical properties of the polymer nanostructures are presented with emphasis on size-dependent behaviors. Several potential applications and corresponding challenges of these nanofibers and nanotubes in chemical, optical and bio-sensors, nano-diodes, field effect transistors, field emission and electrochromic displays, super-capacitors and energy storage, actuators, drug delivery, neural interfaces, and protein purification are also discussed.

© 2011 Elsevier Ltd. All rights reserved.

\* Corresponding author. Fax: +86 532 8595 5977.

E-mail addresses: [yunze.long@163.com](mailto:yunze.long@163.com) (Y.-Z. Long), [meng-meng.li@hotmail.com](mailto:meng-meng.li@hotmail.com) (M.-M. Li), [czgu@aphy.iphy.ac.cn](mailto:czgu@aphy.iphy.ac.cn) (C. Gu), [wamx@iccas.ac.cn](mailto:wamx@iccas.ac.cn) (M. Wan), [duvail@cnsr-immn.fr](mailto:duvail@cnsr-immn.fr) (J.-L. Duvail), [zongwen.liu@sydney.edu.au](mailto:zongwen.liu@sydney.edu.au) (Z. Liu), [eezf@ust.hk](mailto:eezf@ust.hk) (Z. Fan).

<sup>1</sup> Fax: +86 532 8595 5977.

<sup>2</sup> Fax: +86 10 8264 9531.

<sup>3</sup> Fax: +86 10 6255 9373.

<sup>4</sup> Fax: +33 2 4037 3991.

<sup>5</sup> Fax: +61 2 9351 7682.

<sup>6</sup> Fax: +852 2358 1485.

## Contents

|   |      |
|---|------|
| 1. Introduction .....   | 1416 |
| 2. Synthesis methods .....  | 1417 |
| 2.1. Hard physical template method .....  | 1417 |
| 2.2. Soft chemical template method .....  | 1418 |
| 2.3. Electrospinning .....  | 1418 |
| 2.4. Nanoimprint lithography or embossing .....   | 1420 |
| 2.5. Directed electrochemical nanowire assembly .....   | 1420 |
| 2.6. Other methods .....  | 1420 |
| 3. Physical properties of conducting polymer nanotubes and nanofibers .....   | 1420 |
| 3.1. Electronic transport properties .....  | 1420 |
| 3.1.1. Approaches to measure conductivity of individual nanotubes/fibers .....  | 1420 |
| 3.1.2. Electrical conductivity vs. diameter and temperature .....   | 1422 |
| 3.1.3. Nonlinear <i>I–V</i> characteristics .....   | 1424 |
| 3.1.4. Nanocontact resistance .....   | 1425 |
| 3.1.5. Magnetoresistance .....  | 1427 |
| 3.2. Magnetic susceptibility of polyaniline and polypyrrole nanotubes/wires .....   | 1428 |
| 3.3. Specific heat capacity of polyaniline nanotubes .....  | 1430 |
| 3.4. Optical properties and optically-related properties: photoconductance, electrochromism and photothermal effect ..... | 1431 |
| 3.5. Mechanical properties .....  | 1432 |
| 3.6. Microwave absorbing property .....   | 1432 |
| 4. Applications of conducting polymer nanotubes and nanofibers .....  | 1432 |
| 4.1. Chemical, optical and bio-sensors .....  | 1432 |
| 4.2. Field effect transistors and diodes .....  | 1433 |
| 4.3. Polymer light-emitting diodes, field-emission and electrochromic displays .....                                      | 1433 |
| 4.4. Energy storage .....   | 1433 |
| 4.5. Drug release and protein purification .....  | 1434 |
| 4.6. Neural interfaces .....  | 1435 |
| 4.7. Actuators and other applications .....   | 1436 |
| 5. Summary and outlook .....  | 1436 |
| Acknowledgements .....  | 1436 |
| References .....  | 1436 |

## 1. Introduction

In the last few decades, there has been significant progress in one-dimensional (1D) nanostructures with nanoscale and molecular scale properties that can satisfy the demands of the 21st century, for example, carbon nanotubes, inorganic semiconducting and metallic nanotubes/wires, conjugated polymer nanofibers/tubes, etc. [1–11]. These nanostructures have a deep impact on both fundamental research and potential applications in nanoelectronics or molecular electronics, nanodevices and systems, nanocomposite materials, bio-nanotechnology and medicine [1–11].

Semiconducting and metallic polymers are the fourth generation of polymeric materials. Their electrical conductivities can be increased by many orders of magnitude from  $10^{-10}$ – $10^{-5}$  to  $10^2$ – $10^5$  S/cm upon doping [10,11], which cover the whole insulator-semiconductor-metal range. Due to their special conduction mechanism, unique electrical properties, their reversible doping/dedoping process, their controllable chemical and electrochemical properties and their processability, a variety of conducting polymers (e.g., polyacetylene, polyaniline (PANI), polypyrrole (PPY), poly(*p*-phenylene-vinylene) (PPV), poly(3,4-ethylene dioxythiophene) (PEDOT) and other polythiophene derivatives, etc.), especially their 1D nanostructures such as nanotubes and nanowires, have recently received special attention in the areas of nanoscience and nanotechnology [6–11].

Conducting polymer (CP) nanotubes and nanowires can be prepared by physical approaches like electrospinning, chemical routes like hard physical template-guided synthesis and soft chemical template synthesis (e.g., interfacial polymerization, template-free method, dilute polymerization, reverse emulsion polymerization, etc.), and a variety of lithography techniques. As shown in Table 1, each of the established methods possesses advantages and disadvantages, but large scale production of well aligned arrays of CP with controllable morphologies and sizes is still a challenge, although the template method can be a candidate. By now, numerous publications have demonstrated that these one-dimensional polymer nanostructures are promising materials for fabricating polymeric nanodevices such as chemical and bio-sensors, field-effect transistors, field emission and electrochromic display devices, supercapacitors, etc., and exhibit clear advantages over their bulk counterparts in many types of applications. Some good reviews on synthesis methods and applications of CP nano-materials can be found in Refs. [6–14].

In order to fulfill the potential applications of CP nanostructures, it is necessary to precisely address their physical properties. Electrical and optical properties of non-individual 1D-CP nanostructures, have been extensively studied, showing unusual physical and chemical behavior due to the nanosize effects [15,16]. However, this can result in averaging effects or matrix-induced effects which may overcome the intrinsic properties of individual nanowires. There are still some key questions to be

**Table 1**  
Synthesis methods of conducting polymer nanotubes and nanofibers.

| Synthesis methods   | Advantages  | Disadvantages   | Examples   | References  |
|---|---|---|--|-------------|
| Hard Physical Template Method<br>Porous membranes           | Aligned arrays of tubes and wires with controllable length and diameter   | A post-synthesis process is needed to remove the template   | PANI, PPY, P3MT, PEDOT, and PPV nanotubes/wires, CdS-PPY, Au-PEDOT-Au nanowires, MnO <sub>2</sub> /PEDOT and Ni/PPV coaxial nanowires  | [17–31]     |
| Other hard templates  |   |   |  | [32–44]     |
| Soft Chemical Template Method<br>Interfacial polymerization | Simple self-assembly process without an external template   | Relatively poor control of the uniformity of the morphology (shape, diameter); poorly or non-oriented 1D-nanostructures | A variety of PANI and PPY micro/nanostructures such as tubes, wires/fibers, hollow microspheres, nanowire/tube junctions and dendrites | [45,46]     |
| Dilute polymerization                                       |   |   |  | [47]        |
| Template-free method  |   |   |  | [8,9,48,49] |
| Rapidly mixed reaction                                      |   |   |  | [50]        |
| Reverse emulsion polymerization                             |   |   |  | [51]        |
| Ultrasonic shake-up   |   |   |  | [52]        |
| Radiolytic synthesis  |   |   |  | [53–55]     |
| Electrospinning   | Mass fabrication of continuous polymer fibers   | Usually in form of nonwoven web; possible alignment   | PANI/PEO, PPY/PEO, PANI, PPY, P3HT/PEO   | [65–76]     |
| Nanoimprint Lithography or Embossing                        | Rapid and low-cost  | A micro-mold is needed  | PEDOT nanowires, 2D nanodots of semiconducting polymer, and aligned CP arrays  | [77–79]     |
| Directed Electrochemical Nanowire Assembly                  | Electrode-wire-electrode or electrode-wire-target growth of CP micro/nanowires  | Micro/nanowires with knobby structures  | PPY, PANI, and PEDOT nanowires   | [81–86]     |
| Others  | Dip-pen nanolithography method, molecular combing method, whisker method, strong magnetic field-assisted chemical synthesis, et al. |   |  | [87–90]     |

clarified, for example, the effects of the nanocontacts on the electrical measurements, the tuning and the control of the electrical properties of individual nanofibers and nanotubes, etc. These questions are particularly important to develop nanodevices based on individual nanowires and nanotubes. Therefore, in this article, besides synthesis approaches and applications, we also provide a brief review of recent advances in the studies of electronic transport properties, magnetic susceptibility, and specific heat capacity, optical and mechanical properties of nanostructures of conducting polyaniline, polypyrrole and PEDOT based on our results and some important contributions of other groups. All these recent investigations contribute significantly to identify and to understand the specific behavior and applications of conjugated polymer nanostructures in comparison to the bulk materials.

## 2. Synthesis methods

### 2.1. Hard physical template method

The template method of polymerization proposed by Martin et al. [17–25] is an effective technique to synthesize arrays of aligned polymer micro-/nanotubes and wires with controllable length and diameter (as shown in Fig. 1). The disadvantage of this method is that a post-synthesis process is needed in order to remove the template. Many porous materials have been and

are currently being used as templates for the fabrication of nanofibers and tubes, but anodic aluminum oxide (AAO) templates and particle track-etched membranes (PTM) are the most commonly used nanoporous materials. By now, nanotubes/wires of a variety of CPs such as polyaniline [17,18], polypyrrole [17–21], poly(3-methylthiophene) (P3MT) [20], PEDOT [19,22], PPV [25] have been chemically or electrochemically synthesized inside the pores of these membranes. Furthermore, CdS-PPY heterojunction nanowires [26,27], multi-segmented Au-PEDOT-Au and Au-PEDOT-PPY-Au nanowires [28,29], MnO<sub>2</sub>/PEDOT [30] and Ni/PPV [31] coaxial nanowires have also been prepared by the hard template method. For example, core-shell Ni/PPV nanowires were fabricated by a two-step process: tubular PPV shells were prepared first within nanoporous membranes by a wet-chemical technique; the PPV tubules then were operated as a secondary template for the electrodeposition of the Ni cores [31]. The coaxial MnO<sub>2</sub>/PEDOT nanowires were obtained by a simple one-step method of coelectrodeposition in a porous alumina template, the phase segregation of these two materials may help formation of the core-shell structures [30].

Besides these hard templates with channels inside pores, many kinds of pre-existing nanostructures can serve as seeds or templates to synthesize CP nanostructures. For example, polyaniline, polypyrrole, and PEDOT nanofibers/tubes have been prepared by using V<sub>2</sub>O<sub>5</sub>

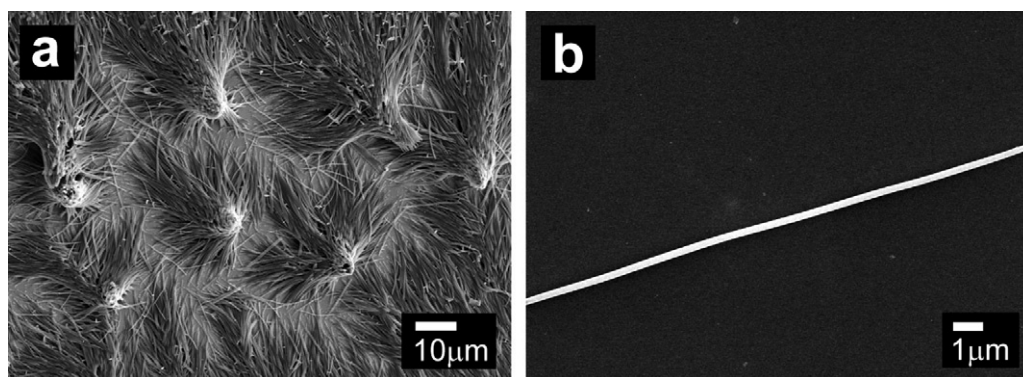


**Fig. 1.** SEM images of PEDOT nanowires anchored on Au thin film (a) or dispersed on a SiO<sub>2</sub>/Si wafer (b), which were synthesized in hard template of polycarbonate track-etched membranes (membranes have been removed).

nanofibers [32–34] or MnO<sub>2</sub> nanowires [35] as seeds. In addition, poly(styrene-*block*-2-vinylpyridine) diblock copolymers [36] and a variety of biological templates such as DNA [37–39] and tobacco mosaic virus [40] have also been used to fabricate conducting polymer nanofibers. Particularly, Abidian et al. [41–44] recently developed a method for the fabrication of PEDOT and polypyrrole nanotubes from biodegradable electrospun nanofibers as templates for drug delivery and neural interface applications.

## 2.2. Soft chemical template method

The soft-template method is another powerful and popular technique to produce CP nanomaterials. By now, surface micelles, surfactants, colloidal particles, liquid-crystalline phases, structure-directing molecules, and aniline oligomers have served as soft templates, and various soft-template methods have been developed: interfacial polymerization [45,46], dilute polymerization [47], template-free method [8,9,48,49], rapidly mixed reactions [50], reverse emulsion polymerization [51], ultrasonic irradiation [52], and radiolytic synthesis [53–55]. The interfacial polymerization method proposed by Kaner et al. [45,46] involves step polymerization of two monomers or agents, which are dissolved respectively in two immiscible phases so that the reaction takes place at the interface between the two liquids. These methods are usually based on self-assembly mechanisms due to hydrogen bonding,  $\pi$ - $\pi$  stacking, van der Waals forces, and electrostatic interactions as driving forces. The disadvantage of the soft-template method is poor control of the morphology, orientation, and diameter of the 1D CP nanostructures.

The template-free method developed by Wan et al. [8,48,49,56–63] is a simple self-assembly (soft-template) method without an external template. By controlling synthesis conditions, such as temperature and molar ratio of monomer to dopant, polyaniline and polypyrrole nanostructures can be prepared by *in situ* doping polymerization in the presence of protonic acids as dopants (as shown in Fig. 2). In the self-assembled formation mechanism in this approach the micelles formed by dopant and/or monomer-dopant act as soft templates in the process of forming tubes/wires [48]. Up to now, a variety of polyaniline

micro/nanostructures such as micro/nanotubes [49,56,57], nanowires/fibers [58–60], hollow microspheres [61,62], nanotube junctions and dendrites [56,63] have been prepared by the template-free method. Furthermore, it was reported that the magnetic and optical properties of polymer micro/nanostructures synthesized by this method can be significantly improved by using a functional dopant (e.g., Fe<sub>3</sub>O<sub>4</sub>,  $\gamma$ -Fe<sub>2</sub>O<sub>3</sub>, carbonyl iron, CoFe<sub>2</sub>O<sub>4</sub> and TiO<sub>2</sub> nanoparticles, azobenzene sulfuric acid, and Rhodamine B, etc.) [8]. Namely, (electrical, magnetic, optical, etc.) multifunctionalized micro/nanostructures of polyaniline can be fabricated by this approach. In addition, self-assembled polyaniline microstructures with high orientation were also reported [64].

## 2.3. Electrospinning

Electrospinning is an effective approach to fabricate long polymer fibers with diameter from micrometers down to 100 nm or even a few nanometers by using strong electrostatic forces [65,66]. As shown in Fig. 3, in the usual electrospinning process, polymer solution is extruded from an orifice to form a small droplet in the presence of an electric field, and then the charged solution jets are extruded from the cone. Generally the fluid extension occurs first in uniform, and then the straight flow lines undergo vigorous whipping and/or splitting motion due to fluid instability and electrically driven bending instability. Finally, the spun fibers are deposited commonly as a nonwoven web on a collector. Through an improved or modified electrospinning device, nanofibers with part or even good orientation could be fabricated [65,66]. By now, micro- and nano-scale fibers of polyaniline/polyethylene oxide (PEO) [67,68], polypyrrole/PEO [68], pure polyaniline [69] and polypyrrole [70,71], poly(3-hexyl-thiophene)/PEO [72], and polyaniline/PEO/carbon nanotubes [73] have been prepared by this technique. In addition, field-effect transistor [74,75] and chemical sensor [76] based on individual electrospun nanofibers have also been reported. Compared with other synthetic approaches, the electrospinning process seems to be the only method that can mass-produce continuous long nanofibers. However, in order to assist in the fiber formation, some non-conducting polymers or chemicals (e.g. PEO) are usually added into

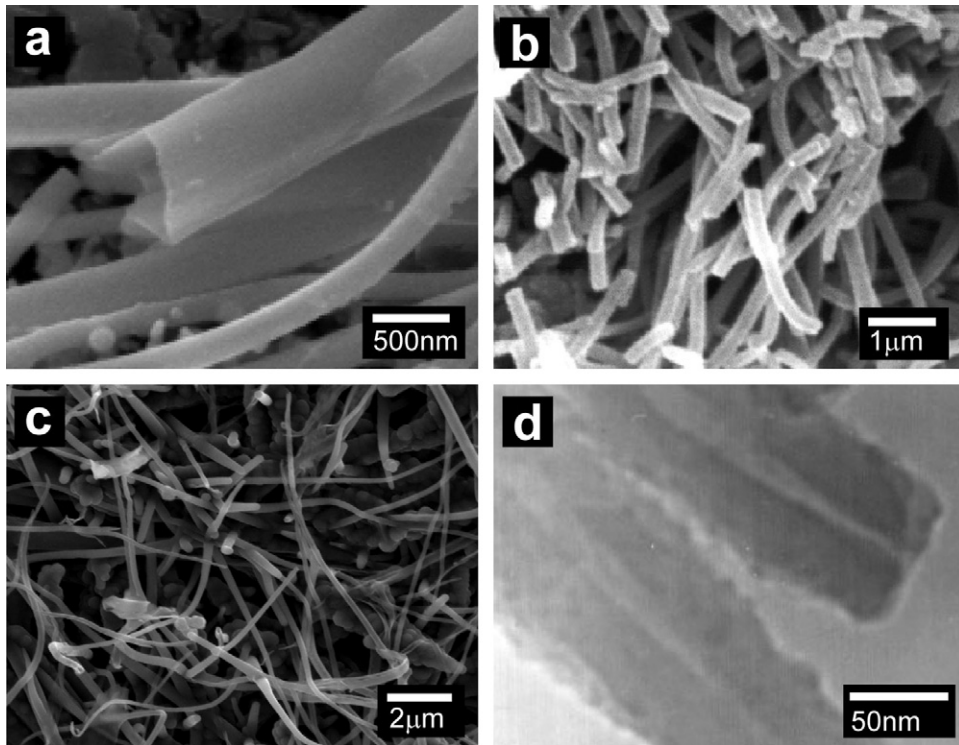


Fig. 2. SEM images of polyaniline nanotubes (a and b), polypyrrole nanotubes (c), and TEM image of polyaniline nanotubes (d), all synthesized by template-free method.

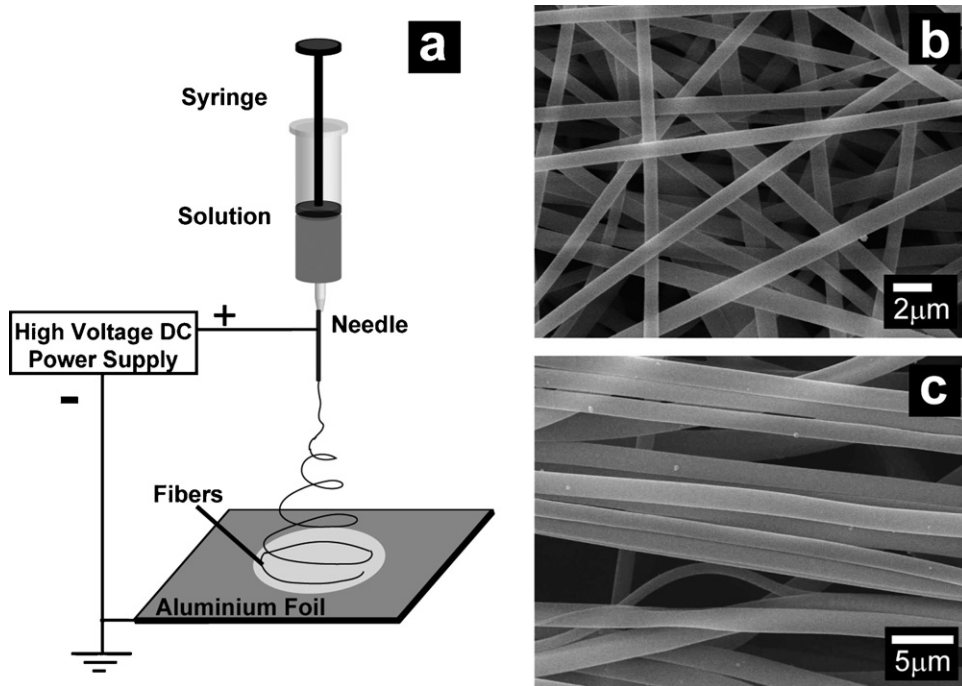


Fig. 3. (a) Schematic diagram of electrospinning method and SEM images of electrospun polymer nanofibers (b) without orientation and (c) with preferential orientation.

spinning solution, which may result in a decrease of the conductivity ( $\sim 10^{-1}$ – $10^{-4}$  S/cm [67,69–71]) of the electrospun composite fibers. It is found that through reducing or eliminating PEO content [69–71,74] or embedding carbon nanotubes in the fibers [73], their conductivity could be increased by one or several orders of magnitude.

#### 2.4. Nanoimprint lithography or embossing

Soft lithography or embossing is a rapid and low-cost approach to shape an initially flat polymer film by using a micro-mold with the assistance of temperature or solvent vapors. Recently, it was reported that conducting polymer nanowires can easily be fabricated by this technique [77–80]. For example, conducting PEDOT doped with poly(4-styrenesulfonate) was patterned in the form of nanowires on a glass or a Si wafer by micro-molding in capillaries [77]. Nanowires and two-dimensional nanodots of semiconducting polymer were also achieved by a liquid embossing technique [77]. In addition, Hu et al. [78] demonstrated that arrays of CP nanowires with internal preferential alignment can be produced by a simple embossing protocol. Recently, Huang et al. [79] proposed a technique based on nanoimprint lithography and a lift-off process for patterning CPs.

#### 2.5. Directed electrochemical nanowire assembly

Directed electrochemical nanowire assembly technique has been employed to grow metal nanowires [81] as well as CP micro/nanowires [82–86]. In this method, CP wire is electrochemically polymerized and assembled onto two biased electrodes (anode and cathode) immersed in aqueous monomer solutions. The essence of this method is an electrode-wire-electrode or electrode-wire-target assembly. Directional growth of polypyrrole, polyaniline, and PEDOT micro/nanowires with knobby structures (e.g., varying from 90 to 700 nm in thickness with a lengthwise averaged diameter of 340 nm for PEDOT wire [86]) between electrodes by this technique was reported recently [82–86]. It was found that these assembled polymer wires can be used as pH sensors [82] and in cell stimulation studies [86].

#### 2.6. Other methods

Some other methods were also reported to produce CP micro/nanostructures. For example, Noy et al. [87] reported the fabrication of luminescent nanostructures and conductive polymer nanowires of controlled size using dip-pen nanolithography. Conducting polymer nanowires of poly(styrenesulfonate) doped PEDOT with diameters under 10 nm were prepared by a molecular combing method [88], which is a well-known technique to stretch a single DNA molecule on various substrates. Recently, Samitsu et al. reported the production of self-assembled conducting polymer nanofibers by a whisker method using anisotropic crystallization in a nematic liquid crystal, and obtained large-scale alignment of the nanofibers [89]. In addition, nanowires consisting of poly(3-hexylthiophene) with part magnetic orientation were prepared by using strong magnetic field [90].

### 3. Physical properties of conducting polymer nanotubes and nanofibers

#### 3.1. Electronic transport properties

##### 3.1.1. Approaches to measure conductivity of individual nanotubes/fibers

In order to fulfill the potential applications of CP nanotubes and fibers, it is necessary to understand the electronic transport properties of individual polymer tubes/fibers. The electrical characterization of individual CP nanotubes/fibers has made significant progress especially during the last decade. The different strategies for estimating or measuring the electrical conductivity of individual nanofibers and nanotubes are reviewed here. It can be mentioned that each approach has its shortcoming, as discussed below.

For template-prepared nanofibers, the easiest and usual way is to leave the synthesized polymer fibers inside the pores of the template membrane and measure the bulk resistance across the filled membrane by a two-probe method [17–23]. Provided the number and diameter of the fibers are known, and assuming the resistance of the membrane is much larger than the parallel sum of the resistances of the CP fibers and thus can be neglected, the measured trans-membrane resistance can be used to estimate the conductivity of a single fiber. It was found that the room-temperature conductivity of 30-nm polypyrrole and poly(3-methylthiophene) fibers [18] and 10-nm PEDOT fibers [19] measured by this method can reach  $2.2 \times 10^3$ ,  $1.68 \times 10^3$  and 780 S/cm, respectively, which are much higher than in conventional forms (e.g. powders or thin films) of the analogous polymer. However, this two-probe resistance measurement method may result in huge uncertainties on values due to the unknown number of connected fibers, to the contact resistance between the conductive paint and the CP thin film lying at the membrane surface, and to the pressure applied on the contact probes [19].

Another way is to measure the resistances of compressed pellet or films (membrane removed) of the polymer nanofibers. Martin et al. [91–93] developed a procedure for making thin films from the template-synthesized polymer tubes and fibers. A four-point conductivity measurement was used on these thin films. These four-point measurements also show that the template-synthesized materials are significantly more conductive. For example, the room-temperature conductivity for polyaniline thin film made from 100-nm tubes is 50 S/cm, whereas bulk conductivity of polyaniline is 9 S/cm [91]. In addition, electrical conductivities of compressed pellets made of polyaniline and polypyrrole nanotubes/wires prepared by the template-free method were also reported by this approach, in the magnitude of  $10^{-2}$ – $10^0$  S/cm [94,95]. However, this approach cannot exclude the inter-fiber contact resistance, which may be larger than the intrinsic resistance of the polymer fibers and even dominate the measured resistance of the compressed pellet or film [23,96].

In fact, the above two methods did not realize the conductivity measurement of an individual fiber directly.

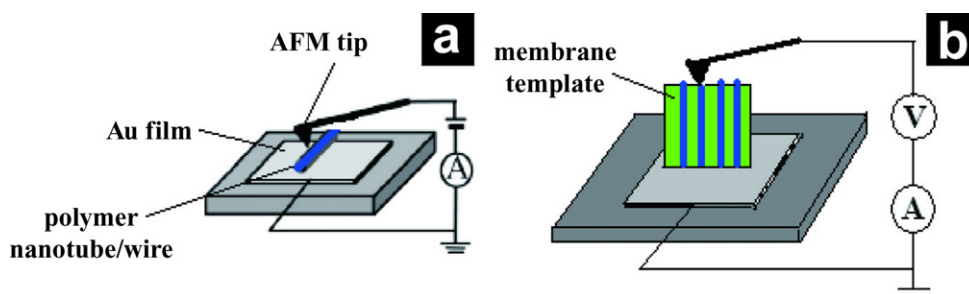


**Fig. 4.** Schematic diagrams of measuring methods of electrical conductivity of individual polymer nanotubes/wires based on a conductive tip of an AFM in both lateral and vertical electrodes configuration.

Recently, the conductivity measurement of single polymer nanotube/wire was achieved based on a conductive tip of an atom-force microscope (AFM) [97–102], as shown in Fig. 4. For example, direct  $I$ – $V$  measurements of isolated polypyrrole nanotube deposited on Au were done using a metal-coated AFM tip. It was found that the resistance is decreased as the contact force is increased and the electrical conductivity of the 120-nm polypyrrole tube has been estimated at about 1 S/cm [97,98]. Saha et al. [99] investigated the current distribution over the selected area of the membrane and the  $I$ – $V$  characteristics of a single polypyrrole nanotube by this approach. They reported that the intrinsic conductivity of the polypyrrole tube changes with the wall thickness, and the conductivity for tubes with a wall thickness of 15 nm can reach about 5000 S/cm [99]. For comparison, the room-temperature conductivity of individual polyaniline nanotubes determined by this approach is in the range of 0.1–15 S/cm [100,101]. It is worth noting that in this two-probe geometry, the contact resistance cannot be excluded but can be minimized by applying a significant pressure of the tip onto the nanotube/wire [97,98].

A common approach was generally realized by dispersing nanotubes/wires on patterned micro- or nano-electrodes prepared by photo-lithography, electron-beam lithography or focused-ion beam deposition, followed by the subsequent searching of nanofibers just lying on only two, three or four electrodes [14,24,28,29,67,68,74,88,103–108], as shown in Fig. 5. For example, electrical conductivity ( $\sigma_{RT} \sim 417$  S/cm), magnetoresistance and  $I$ – $V$  characteristics of iodine-doped polyacetylene fiber network and nanofibers were measured by this approach [103]. The conductivity of a single 1320-nm polyaniline/PEO (72 wt% PANI in PEO) fiber prepared by electrospinning was measured to be 33 S/cm at 295 K [67,68]. The conductivity of two single PEDOT nanowires with diameters under 10 nm was determined by this method to be 0.6 and 0.09 S/cm [88]. However, nanocontact resistance between the pre-patterned metal micro-electrodes and the dispersed polymer fiber is uncertain and often shows large sample-to-sample variations. Additional treatments may be needed to promise a good contact. Another problem for this approach often occurs: two or many isolated fibers cross over the same patterned electrodes [74,88]. In this case, some fibers crossed over the electrodes may be cut off with AFM manipulation [88].

In recent years, focused-ion beam (FIB) assisted deposition technique has been employed to attach

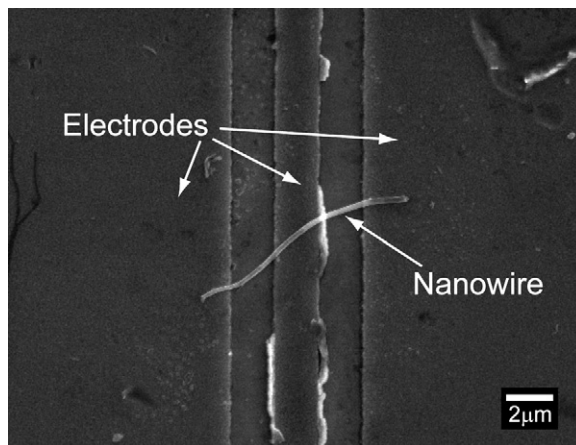


**Fig. 5.** SEM image of a single polypyrrole nanowire crossed over the pre-patterned metal electrodes.

metal microleads on isolated nanotubes/wires directly [57,96,109–116]. Fig. 6 shows an isolated polyaniline nanotube and attached platinum microleads, which were fabricated by FIB assisted deposition. The directly measured four-probe conductivity of the single polyaniline tube is about 31 S/cm [109], which is much higher than the bulk conductivity of the polyaniline tube pellet (about 0.035 S/cm). Electrical properties of individual polypyrrole tubes [110] and PEDOT wires [111] with different diameters were also reported by using this approach. Generally, platinum microlead fabricated by FIB assisted deposition

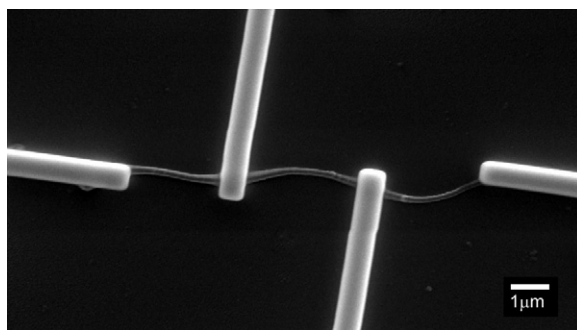


**Fig. 6.** SEM image of an isolated polyaniline nanotube and attached platinum microleads by FIB deposition [109]. Copyright 2003 American Institute of Physics.

can promise a solid and ohmic contact to the fiber [117]. However, in order to minimize the possible modification or damage of the polymer fiber due to the incoming gallium ions, very low focused-ion beam currents ( $I = 1\text{--}30\text{ pA}$ ) should be used [111].

In addition, a directed electrochemical nanowire assembly technique has been recently developed. It consists in the growth of CP micro/nanowires between patterned electrodes [82–86]. It was found that the conductivity of the polymer wires grown and measured by this approach is about  $0.5\text{ S/cm}$  for the polypyrrole wires and about  $7.6\text{ S/cm}$  for the polythiophene wires [86]. Lee et al. reported that the conductivity of polyaniline wires with diameter of  $133\text{ nm}$  can reach about  $4200\text{ S/cm}$  [85]. Yun et al. also demonstrated that the electrochemically grown polypyrrole wires can be used for individually addressable pH sensor arrays [82]. An obvious advantage of this approach is that the conductivity measurement of a single wire is possible on the as-synthesized nanofiber, which avoids additional lithographic process. Here, it should be noted that the conductivity measured by this approach can only be obtained by two-probe geometry, because the polymer wires are grown between the selected two (anode and cathode) electrodes.

The above results indicate the electrical conductivity of CP nanotubes/fibers has been explored by different approaches. The reported conductivity values vary in a wide range from  $10^{-1}$  to  $10^3\text{ S/cm}$  (For reference, the theoretically calculated conductivity parallel to the chain can reach  $2 \times 10^6\text{ S/cm}$  for polyacetylene [11]). Besides the polymer physical structure, the extent of disorder, the fiber diameter, the doping level and the dopant type, the technique used for the conductivity measurement are also key factors and have to be considered for comparing values.

### 3.1.2. Electrical conductivity vs. diameter and temperature

The dependence of room-temperature conductivity on the diameter of the polymer nanotubes/wires has been widely reported since 1989 [17–23,118]. These studies concern nanowires and nanotubes prepared by the hard template method. It was found that the room-temperature conductivities of nanotubes/wires of conducting polypyrrole, polyaniline and polythiophene derivatives can increase from  $10^{-1}$ – $10^0$  to about  $10^3\text{ S/cm}$  with decrease of their outer diameters from  $1500$  to  $35\text{ nm}$ . The mechanism responsible for this effect has been ascribed to the enhancement of molecular and supermolecular ordering with the alignment of the polymer chains, as confirmed by studies on polarized infrared absorption spectroscopy and X-ray diffraction [17,18,20]. For PEDOT nanowires prepared by the hard template method, the room-temperature conductivities of the nanowires with diameters of  $190$ ,  $95$ – $100$ ,  $35$ – $40$ , and  $20$ – $25\text{ nm}$  are about  $11$ ,  $30$ – $50$ ,  $470$ – $520$ , and  $390$ – $550\text{ S/cm}$ , respectively, as shown in Fig. 7a [111]. For polypyrrole nanotubes prepared by the template-free method, it was found that a polypyrrole tube with a  $560$ – $400\text{ nm}$  outer diameter is poorly conductive, with a room-temperature conductivity of only  $0.13$ – $0.29\text{ S/cm}$ , as shown in Fig. 7b. When the outer diameter is decreased to  $130\text{ nm}$ , the conductivity of the

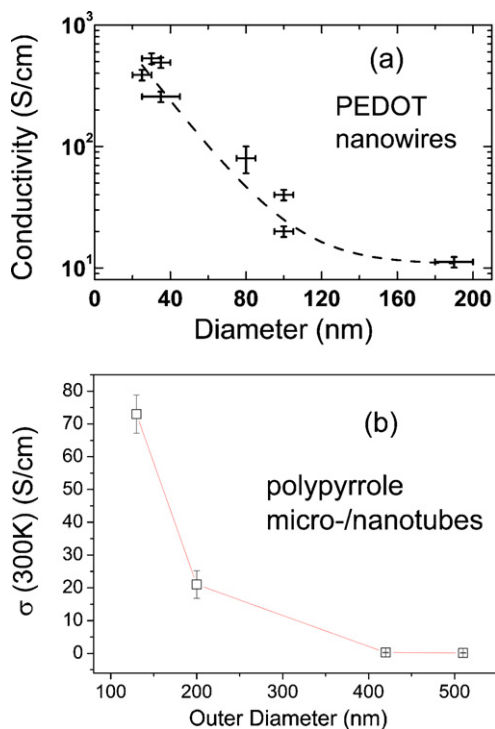


**Fig. 7.** Diameter dependence of room-temperature conductivity of individual (a) hard template- synthesized PEDOT nanowires [111] and (b) template-free self-assembled polypyrrole tubes [110]. Copyright 2007 American Institute of Physics & Copyright 2005 The American Physical Society, separately.

single nanotube increases to  $73\text{ S/cm}$  [110]. Such a conductivity dependence on diameter was observed not only for hard template-synthesized polymer tubes/wires, but also for template-free self-assembled polypyrrole tubes, which indicates that the polymer tubes/wires prepared by these two methods have similar structural characteristic: the smaller the diameter, the better the polymer chain ordering.

Since the electrical properties of polymer are strongly influenced by the effect of disorder and temperature, three different regimes (namely, insulating, critical, and metallic regimes close to the Anderson metal-insulator transition) have been sorted out based on the extent of disorder and conductivity dependence on temperature [15,16,119]. In the insulating regime, for a three-dimensional system, the temperature dependent resistivity usually follows three-dimensional (3D) Mott variable-range hopping (VRH) model:  $\rho(T) = \rho_0 \exp(T_M/T)^{1/4}$ , where  $T_M$  is the characteristic Mott temperature. At lower temperatures, when the Coulomb interaction between charge carriers becomes significant,  $\rho(T)$  usually follows Efros-Shklovskii (ES) VRH:  $\rho(T) = \rho_0 \exp(T_{ES}/T)^{1/2}$ , where  $T_{ES}$  is the characteristic ES temperature. In the critical regime, for a three-dimensional system close to the metal-insulator transition, the resistivity follows a power-law dependence:  $\rho(T) \propto T^{-\beta}$ , where  $\beta$  lies within the range of  $0.3 < \beta < 1$ . In the metallic regime, the sample shows a positive temperature coefficient of the resistivity at low temperatures (for example, below  $10$ – $20\text{ K}$  for metallic polypyrrole films [119]).

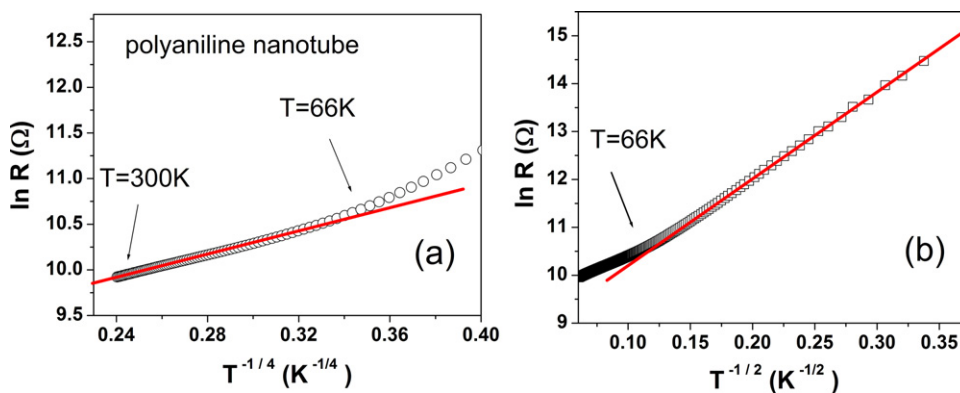


**Fig. 8.** The dependence of resistance on temperature of a single polyaniline nanotube ( $\sigma_{RT} = 47 \text{ S/cm}$ ) in the insulating regime of the metal-insulator transition: (a) plotted as  $\ln R(T)$  versus  $T^{-1/4}$ ; (b) plotted as  $\ln R(T)$  versus  $T^{-1/2}$ ; the temperature dependence of resistance follows 3D-VRH at higher temperatures and follows ES-VRH at lower temperatures [110]. Copyright 2005 The American Physical Society.

Long et al. reported the temperature dependent resistivity of a single polyaniline nanotube with average outer and inner diameters of 120 nm and 80 nm, which falls in the insulating regime of metal-insulator transition [110]. The tube's room-temperature conductivity is 47 S/cm. It was found that the resistivity follows 3D Mott-VRH above 66 K, and follows ES-VRH model below 66 K, as shown in Fig. 8. Here it is noted that from the view point of charge carriers, the polymer tube/wire with an outer diameter of 120 nm is still three dimensional because the localization length of carriers ( $L_C < 20 \text{ nm}$ ) is much smaller than the wall thickness or the diameter of the submicrotube. Similar smooth crossover from Mott-VRH to ES-VRH has also been observed in a single polypyrrole microtube (room-temperature conductivity, 0.8 S/cm) at around 96 K [110]. It is noted that the crossover temperature ( $T_{\text{cros}} \sim 66\text{--}96 \text{ K}$ ) and the characteristic ES temperature ( $T_{\text{ES}} \sim 316\text{--}780 \text{ K}$ ) of a single polymer tube/wire are much higher than that of a polyaniline pellet or a polypyrrole film ( $T_{\text{cros}} < 15 \text{ K}$  and  $T_{\text{ES}} \sim 29\text{--}56 \text{ K}$ ), which could be possibly due to enhanced strong Coulomb interaction in polymer nanotubes/wires at low temperatures. In addition, it is worthy to note that Aleshin et al. reported power-law dependent electrical conductance ( $G(T) \propto T^\alpha$  with  $\alpha \sim 2.2\text{--}7.2$ ) in individual polyacetylene nanofibers and polypyrrole nanotubes possibly owing to repulsive short-range electron-electron interactions [14,107].

In addition, with the decrease of disorder or diameter of polymer nanotubes/wires, the room-temperature conductivity of 73 S/cm found with the 130-nm polypyrrole nanotube is close to the critical regime of metal-insulator transition [110]. Its resistivity follows the power-law dependence:  $\rho(T) \propto T^{-\beta}$ , as shown in Fig. 9a. The fit yields a  $\beta$  value of 0.49. Duval et al. reported that two-different 100-nm PEDOT nanowire ( $\sigma_{RT} \sim 50 \text{ S/cm}$ ) fell in the critical regime with a  $\beta$  value of about 0.78 [111]. Furthermore, the 35–40 nm template-prepared PEDOT nanowire ( $\sigma_{RT} \sim 490 \text{ S/cm}$ ) displays a metal-insulator transition at about 32 K, as shown in Fig. 9b, indicating that the nanowire is in the metallic regime of the metal-insulator transition [111]. However, for a PEDOT nanowire with a diameter of 20–25 nm, and high room-temperature conductivity

( $\sim 390\text{--}550 \text{ S/cm}$ ), a very strong temperature dependence ( $R(10 \text{ K})/R(300 \text{ K}) \sim 10^5$ ) and an insulating behavior at low temperature have been measured. This is possibly due to a confining effect since the value of the diameter (20–25 nm) is equal or close to the localization length of electrons ( $L_C \sim 20 \text{ nm}$ ). In such a case, localization of electrons induced by Coulomb interaction or small disorder must be taken into account to explain the insulating behavior at low temperatures. It should be noted that for the hard template-synthesized PEDOT nanowires, the

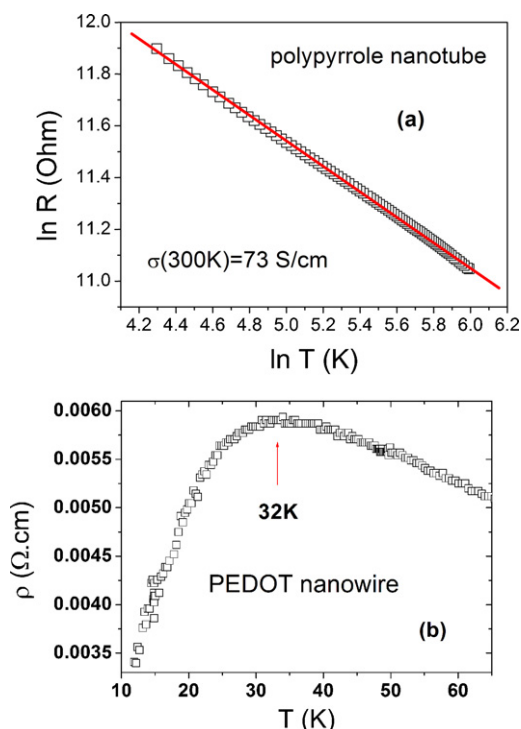


**Fig. 9.** Temperature dependences of resistance for (a) a single 130-nm polypyrrole nanotube in the critical regime [110] and (b) a single 35–40 nm PEDOT nanowire in the metallic regime of metal-insulator transition [111]. Copyright 2005 The American Physical Society & Copyright 2007 American Institute of Physics, separately.

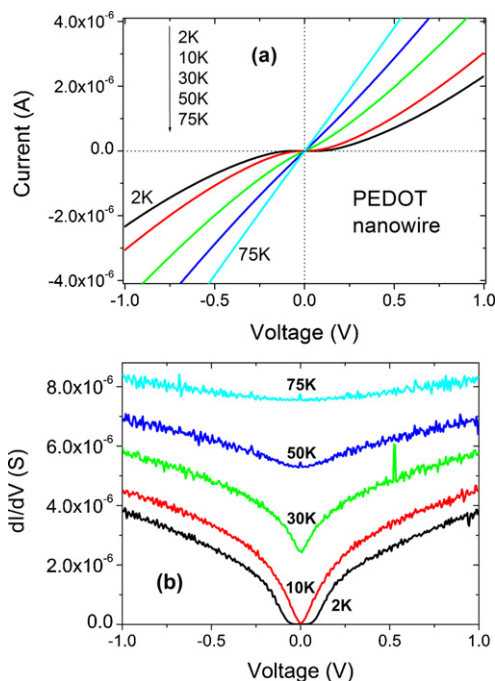


**Fig. 10.**  $I$ - $V$  characteristics (a) and the corresponding differential conductance ( $dI/dV$ ) curves (b) of a single PEDOT nanowire at low temperatures.

temperature dependences of the four-probe resistivity demonstrate that the PEDOT nanowires with diameters of 190, 95–100, 35–40 and 20–25 nm are in the insulating, critical, metallic and insulating regimes of metal-insulator transition, respectively [111]. This result indicates that the electronic transport properties of individual polymer nanowires could be tuned by controlling the diameter.

### 3.1.3. Nonlinear $I$ - $V$ characteristics

The current-voltage ( $I$ - $V$ ) characteristics of individual polymer nanowires/tubes have been explored extensively in the past 10 years [14,28,29,67,68,98–101,103–108,110,116,120–127]. With decreasing temperature, a transition from linear to nonlinear  $I$ - $V$  characteristics is usually observed (Fig. 10a), and a clear zero bias anomaly (i.e., Coulomb gap-like structure) gradually appears on the differential conductance ( $dI/dV$ ) curves (Fig. 10b). Similar transition has also been reported in polyacetylene fibers [105], carbon nanotubes [128], self-assembled wire made of Au nanorods [81], and inorganic compound nanowires such as CdS nanoropes [129],  $K_{0.27}MnO_2$  nanowires [130],  $SnO_2$  [131] and  $ZnO$  [132] nanowires.

Up to now, several theoretical models, such as space-charge limited current [84,104], fluctuation-induced tunneling [122,125], Coulomb gap [110,128,130,131], Coulomb blockade [108,126,129], Luttinger liquid [14,107], and Wigner crystal [14,127] models, have been considered to explain the conduction mechanism of quasi-one dimensional nanofibers. For example, Saha and Aleshin et al. reported single-electron tunneling or Coulomb-blockade transport in conducting polypyrrole and helical polyacetylene nanofibers [108,126], respectively. In addition,

power-law behaviors for both  $I$ - $V$  characteristics ( $I(V) \propto V^\beta$  with  $\beta \sim 2$ –5.7) and electrical conductance ( $G(T) \propto T^\alpha$  with  $\alpha \sim 2.2$ –7.2) have been reported recently in polyacetylene fibers [107] and polypyrrole wires/tubes [127], which is characteristic of one-dimensional systems composed of several Luttinger liquids or Wigner crystals connected in series, owing to electron-electron interactions (repulsive short-range electron-electron interactions or long-range Coulomb interactions). Similar nonlinear transport was also reported in other semiconducting conjugated polymers at high carrier densities [133]. In the Luttinger liquid model,  $I$ - $V$  curves measured at different temperatures should be fitted by the general equation [14,107]

$$I = I_0 T^{\alpha+1} \sinh\left(\frac{eV}{k_B T}\right) \left| \Gamma\left(1 + \frac{\beta}{2} + \frac{iV}{\pi k_B T}\right) \right|^2 \quad (1)$$

where  $\Gamma$  is the Gamma function,  $V$  is the voltage bias, and  $I_0$  is a constant. The parameters  $\alpha$  and  $\beta$  correspond to exponents estimated from the  $G(T)$  and  $I(V)$  plots. Namely, the  $I$ - $V$  curves should collapse into a single curve if  $I/T^{\alpha+1}$  is plotted as a function of  $eV/k_B T$ .

Particularly, Kaiser et al. [122,125] recently proposed a generic expression (extended fluctuation-induced tunneling and thermal excitation model) for the nonlinear  $I$ - $V$  curves based on numerical calculations for metallic conduction interrupted by small barriers:

$$G = \frac{I}{V} = \frac{G_0 \cdot \exp(V/V_0)}{1 + h[\exp(V/V_0) - 1]} \quad (2)$$

where  $G_0$  is the temperature-dependent zero-bias conductance;  $V_0$  is the voltage scale factor, which strongly depends on the barrier energy;  $h = G_0/G_h$  (where  $h < 1$ ), which yields a decrease of  $G$  below the exponential increase at higher values of voltage  $V$  (the saturation of  $G$  at a high-field value,  $G_h$ , as  $V \rightarrow \infty$  given by expression (2) is an extrapolation of the calculations). Kaiser et al. showed that this expression gave a very good description of the observed nonlinearities in polyacetylene nanofibers, vanadium pentoxide nanofibers, etc. [122,125]. Here, one can wonder whether the Kaiser expression is appropriate to fit the nonlinear  $I$ - $V$  characteristics of individual polymer nanowires/tubes if the Coulomb interactions are strong and should be taken into account.

The Kaiser expression has been used by Long et al. [116,134] to numerically calculate the  $I$ - $V$  characteristics of individual polyaniline nanotube, polypyrrole nanotubes, PEDOT nanowires, CdS nanorope, and  $K_{0.27}MnO_2$  nanowire. As shown in Fig. 11, the results indicate that except at low temperatures and low bias voltages, the Kaiser generic expression can give a good description of the  $I$ - $V$  characteristics of individual nanotubes/wires. This indicates that the Kaiser expression (extending the Sheng model or fluctuation-induced tunneling and thermal excitation model) takes into account the microstructure feature and the conduction feature of polymer nanofibers (quasi-one-dimensional metallic conduction interrupted by small barriers). However, apparent deviation from the Kaiser expression has been evidenced in the low-temperature  $I$ - $V$  curves (Fig. 11).

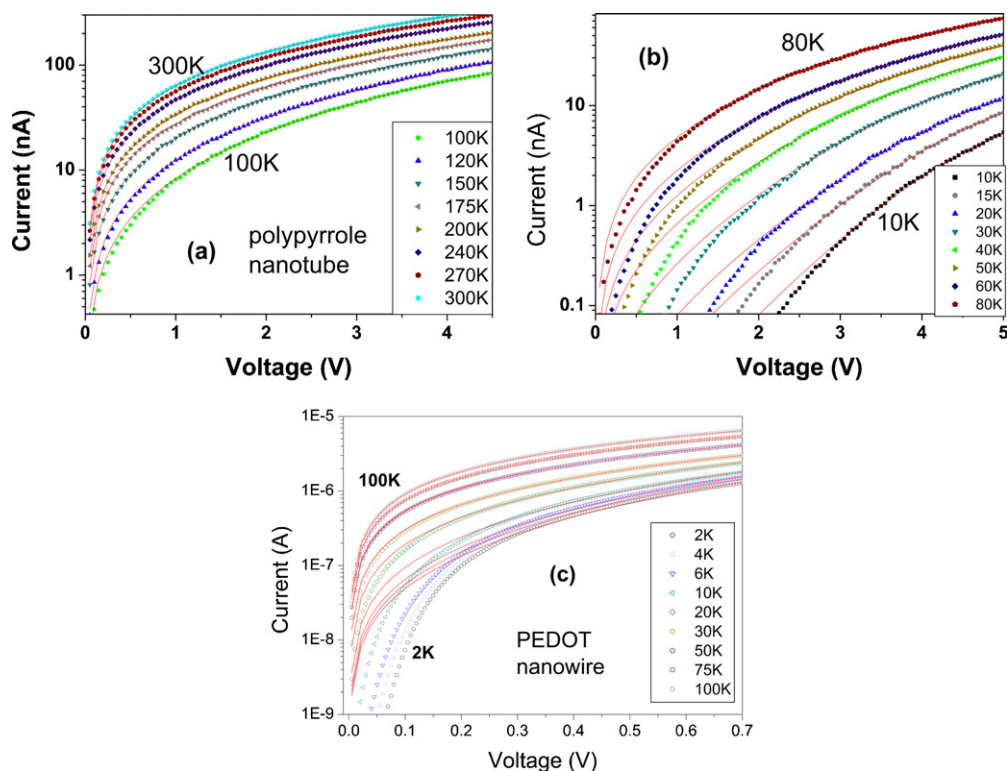


**Fig. 11.**  $I$ - $V$  characteristics of a single polypyrrole nanotube, also showing the fits by expression (2), at temperatures (a) ranging from 300 to 100 K and (b) from 80 to 10 K, and a single PEDOT nanowire with fits to expression (2) at temperatures ranging from 100 to 2 K [116]. Copyright 2009 Chinese Physical Society and IOP Publishing Ltd.

In particular, we compare the values of zero-bias conductance determined from the fitting parameter  $G_0$  with that determined from experimental measurements ( $G_0'$ , obtained from the  $I$ - $V$  curve or the differential conductance). As shown in Fig. 12, the  $G_0$  decreases smoothly with temperature lowering, but the experimental value  $G_0'$  sharply decreases below 80–100 K and deviates from  $G_0$ ,

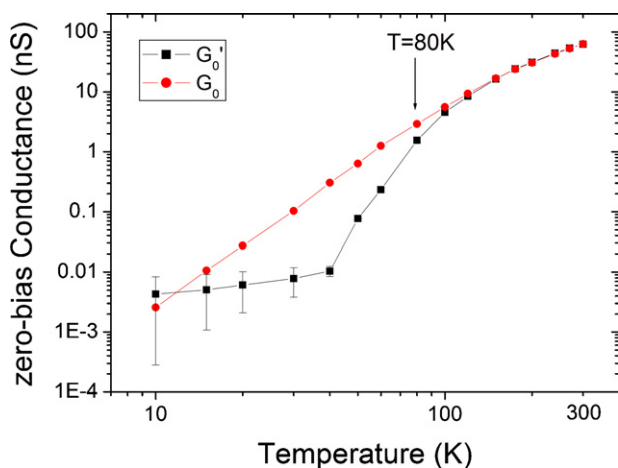


**Fig. 12.** Variation of the zero-bias conductance with temperature varying, where  $G_0$  is determined from the fitting data and  $G_0'$  is determined from the experimental data of the single polypyrrole nanotube [116]. Copyright 2009 Chinese Physical Society and IOP Publishing Ltd.

although superposes with  $G_0$  for temperature equal and larger to 100 K. We note that the deviation temperature (about 80 K) is consistent with the crossover temperature (66–96 K) for the cross-over from Mott-VRH to ES-VRH, as shown in Fig. 8. We propose that one possible reason for the deviation is that the Kaiser expression does not include the contributions from the Coulomb-gap occurring in density of states near Fermi level and/or enhanced Coulomb interactions due to nanosize effects, which become important at low temperatures and voltages [110,116,134].

### 3.1.4. Nanocontact resistance

The contact resistance is often encountered in studies of the electronic transport of an individual polymer nanowire/tube or polymer nanofiber-based nanodevices. As we know, there are two major factors responsible for the contact resistance magnitude: geometry and insulating layers (or potential barriers) between the contacting surfaces. From the geometrical point of view, and considering an homogeneous contact over the whole contact area, the resistance of a contact is inversely proportional to its area, and is dependent on the surface stiffness and the force holding the two surfaces together. Particularly, the relative energy shifts of the Fermi level of the polymer nanowire and the metal electrode may lead to formation of a diode, p-n junction or metal-semiconductor junction due to their different energy levels or work functions. In addition, insulating layer on the unclean surfaces (residual layer due to the contact processes) may be critical when the

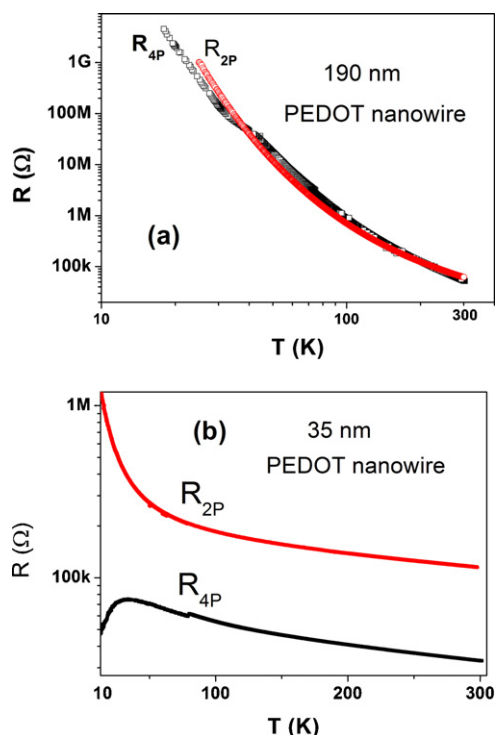


**Fig. 13.** The temperature dependence of the four-probe resistance ( $R_{4P}$ ) and the two-probe resistance ( $R_{2P}$ ) of (a) an individual PEDOT nanowire with a diameter of 35 nm, which falls in the metallic regime of the metal-insulator transition, and (b) an individual PEDOT nanowire with a diameter of 190 nm, which falls in the insulating regime of the metal-insulator transition [135]. Copyright to the authors 2009.

contact size is very small. A bad (insulating or semiconducting) electronic contact may possess a strongly temperature dependent contact resistance, and thus can seriously complicate or even dominate the measured resistance. In this section, we discuss two kinds of nanocontact resistance: between polymer nanowire/tube and metal microlead and between two crossed polymer nanowires/tubes.

The nanocontact resistance between a polymer PEDOT nanowire and a platinum microlead fabricated by focused-ion-beam deposition has also been studied by Long et al. [135]. It was found that the nanocontact resistance (determined from four-probe resistance and two-probe resistance of the same nanowire) is about 10 k $\Omega$  at room temperature and can reach 10 M $\Omega$  at low temperatures, which, in some case, is comparable to the intrinsic resistance of the PEDOT nanowires. On the one hand, for a semiconducting polymer nanowire in the insulating regime of the metal-insulator transition, the four-probe resistance is quite close to the two-probe resistance because the contact resistance is much smaller than the intrinsic resistance of the polymer nanowire as shown in Fig. 13 [135]. On the other hand, for a nanowire that falls in the metallic regime of the metal-insulator transition (for example, the 35 nm PEDOT nanowire as shown in Fig. 13 [135]), the metallic nature of the measured polymer fibers could be overshadowed in the two-probe measurement, although the nanowire shows a relatively high electrical conductivity at room temperature (390–450 S/cm),

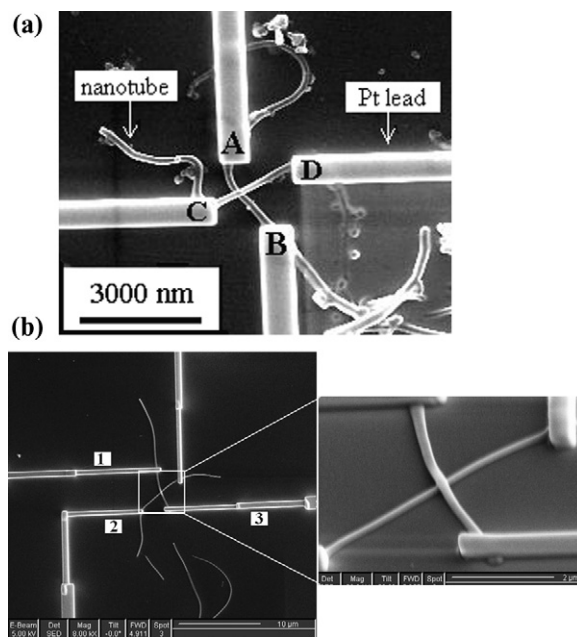


**Fig. 14.** SEM images showing two crossed poly(aniline) nanotubes (a) and two crossed PEDOT nanowires (b) and their attached Pt microleads [96,140]. Copyright 2003 Wiley-VCH Verlag GmbH & Co. KGaA, Weinheim and Copyright 2009 Materials Research Society, separately.

because the nanocontact resistance is much larger than the intrinsic resistance of the nanowire especially at low temperatures. We note that, for individual RuO<sub>2</sub> nanowires [136], the temperature dependence of the two-probe resistance indicates that the nanowire is semiconducting, whereas the four-probe resistance dependence of the same nanowire shows the nanowire is metallic. Nanocontact resistance has also been widely reported in carbon nanotubes and other inorganic semiconductor nanowires [137–139]. So, in order to explore the intrinsic electronic transport properties of individual nanowires, especially in the case of metallic nanowires, the four-probe electrical measurement is required.

The nanocontact resistance between two crossed polymer nanotubes/wires has been studied by Long et al. [96,140]. It was found that the inter-tubular junction resistance of two crossed poly(aniline) nanotubes (Fig. 14) is very large, about 500 k $\Omega$  at room temperature, which is nearly 16 times larger than the intra-tube (intrinsic) resistance of an individual PANI nanotube (about 30 k $\Omega$  for 5- $\mu$ m long nanotube) [96]. This result explains straightforwardly why an individual poly(aniline) nanotube has a much higher room-temperature conductivity (30.5 S/cm) than that of a pellet of poly(aniline) nanotubes where the measured resistance is dominated by the inter-fibrillar resistance (0.03 S/cm). For crossed PEDOT nanowires, the junction resistance (between the two nanowires) at room temperature can vary from 885–1383 k $\Omega$  for one sample to 370–460 M $\Omega$  for another sample, respectively comparable or much larger than the intrinsic resistance of the PEDOT nanowires. In addition, the contact resistance shows a stronger temperature dependence ( $R(72\text{ K})/R(300\text{ K})$  is about 120–141) and could be fitted by a thermal

fluctuation-induced tunneling (FIT) model [140]. It should be noted that the nano-junction resistance is comparable to the intrinsic resistance of polymer nanotube/wire and shows large sample-to-sample variations. Possible reasons could be contamination of the nanotube/wire surfaces from solvent impurities or water adsorption, the variation of the junction area between the two nanotubes/wires, or the self-formation conditions of the junction; no special effort was made to control the formation of the junction between the two crossed nanotubes/wires during fabrication.

### 3.1.5. Magnetoresistance

The magnetoresistance MR (defined as  $MR = \Delta R(H)/R(0) = [R(H) - R(0)]/R(0)$ ) of bulk films of CPs have been extensively studied over the last 20 years [15,16,119]. For example, polyaniline, polypyrrole, PEDOT films, and polyaniline composites usually exhibit a positive magnetoresistance at low temperatures ( $T < 10$  K) and  $MR \propto H^2$  ( $H$  is not very large). The mechanism generally involved is the shrinkage of localized wavefunctions of electrons in the presence of a magnetic field or electron-electron interactions [15,16,119]. Highly conductive polyacetylene films usually show a negative magnetoresistance at low temperatures, generally attributed to the weak localization effects [15,16,141]. Up to date, only a few papers have reported the magnetoresistance of polymer nanotubes/wires [103,105,110,141–145]. Since the individual polymer tubes/wires have a much smaller size (e.g., size effect induced by structural/electronic

changes of CP when synthesized in nanostructures), their magnetoresistance is found to be different from that of the bulk films and pellets.

Long et al. reported that the magnetoresistance of single polyaniline nanotube and single PEDOT nanowire is positive below 10 K and increases as  $H^2$  up to 9 T. [110,142] Typically, a positive magnetoresistance is expected for hopping conduction, because the applied magnetic field contracts the overlap of the localized state wavefunctions and it thus results in an increase of the average hopping length. It corresponds to a positive magnetoresistance at sufficiently low temperatures. The theory of positive magnetoresistance has been developed for two cases, without and with electron-electron interactions. In both cases, the weak-field MR with strong temperature dependence can be expressed as  $\ln(R(H)/R(0)) \propto H^2 T^{-3/4}$  [146]. However, the magnetoresistance of a single nanotube/wire is much smaller than that of the nanotube/wire pellet at 9 T: MR < 5% (2 K) for the single polyaniline nanotube and PEDOT nanowire (Fig. 15a and b), and MR ~ 90% (3 K) for the polyaniline nanotubes' pellet (Fig. 15c) [142]. In addition, when the temperature increases, the magnetoresistance of the single nanotube/wire becomes smaller and close to zero. No evident transition from a positive magnetoresistance to negative one was observed. In contrast to single nanotube/wire, pellets of polyaniline and polypyrrole nanotubes/wires show a relatively large positive magnetoresistance at low temperatures. With temperature increasing, there is a transition from positive magnetoresistance to small negative magnetoresistance at about

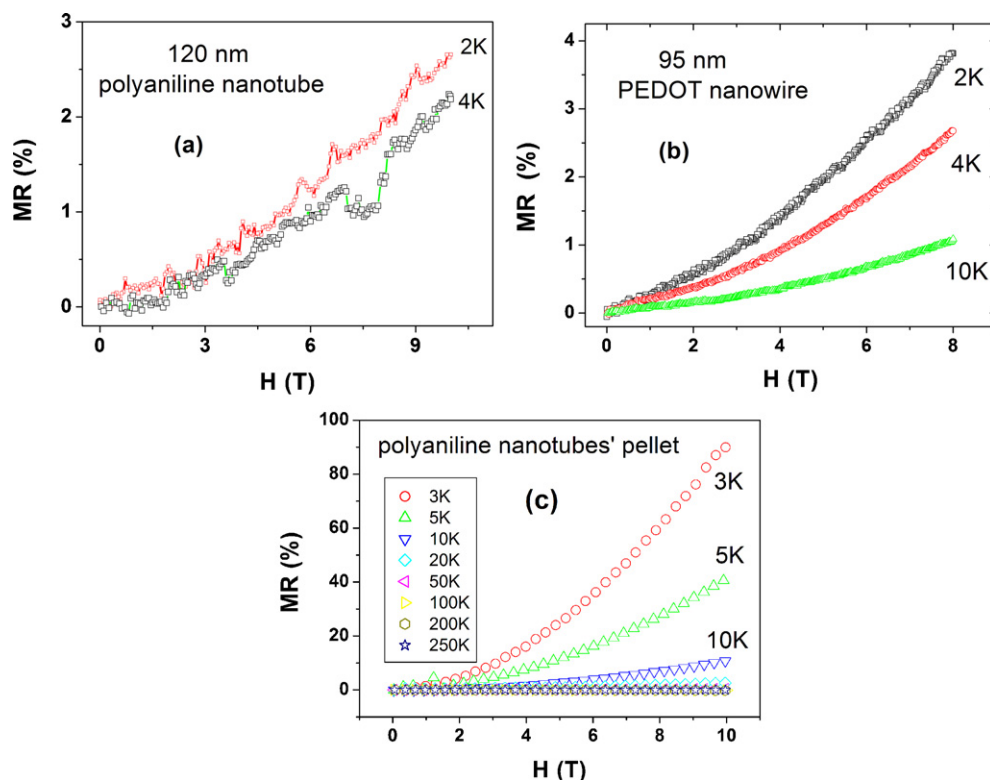


Fig. 15. The magnetoresistance curves for different temperatures of (a) a single polyaniline nanotube, (b) a single PEDOT nanowire, and (c) a pellet of polyaniline nanotubes [142]. Copyright 2006 IOP Publishing Ltd.

60 K. The results indicate that the magnetoresistance in the bulk pellet samples made of polymer nanotubes/wires is dominated by a random network of inter-fibril contacts.

A small magnetoresistance effect in individual polymer nanotube/wire has been confirmed in other samples. For example, the low-temperature magnetoresistance (MR ~ 0.1%) in a polyacetylene nanofiber network is rather smaller than that in a bulk polyacetylene film [103,105]. A vanishing MR of polyacetylene nanofibers in high electric fields has also been reported recently [145]. In addition, a single gold/polyaniline microfiber shows a small positive magnetoresistance (MR < 4.1%) below 6 K [143]. The reason for this weak magnetoresistance effect in individual polymer nanotube/wire is possibly due to the elimination of inter-nanotube/wire contacts, small size and, relatively high conductivity of individual polymer nanotube/wire [105,142]. The vanishing MR of polyacetylene nanofibers in high electric fields is ascribed to the deconfinement conduction of spinless charged solitons [145].

### 3.2. Magnetic susceptibility of polyaniline and polypyrrole nanotubes/wires

Since the magnetic properties can provide important details of charge-carrying species and unpaired spins, magnetic susceptibility of CPs such as polyacetylene, polyaniline, polypyrrole, and polythiophene has been extensively studied [147–159]. It was found that the total dc magnetic susceptibility ( $\chi_{dc}$ ) of doped polymer could be separated into three components: atomic core diamagnetism  $\chi_{dia}$ , local-moment Curie-law paramagnetism  $\chi_C = C/T$  (where  $C$  is the Curie constant), and temperature-independent Pauli paramagnetism  $\chi_P$ :  $\chi_{dc} = \chi_{dia} + \chi_C + \chi_P = \chi_{dia} + \chi_P + C/T$ . The magnetic susceptibility clearly changes from a Curie-like to a Pauli-like behavior as the temperature arises. Through susceptibility studies, the coexistence of polarons and bipolarons in doped polyaniline and polypyrrole has been suggested [149,156]. It should be mentioned that Kahol et al. [150–152] found that nearly all polyaniline derivatives have a nearly linear  $\chi(T)T$  dependence on  $T$ , and pointed out that the simple interpretation of the “linear” part of the  $\chi(T)T$  vs.  $T$  plot in terms of Pauli-like susceptibility may not be correct especially for less conducting polymeric materials, because most of the spins are localized and there are only a low or zero density of states at the Fermi level. For such a disordered system, a pair of polarons (called bipolaron) can be formed by being held together by a strong exchange interaction characterized by the coupling constant  $J$ , the magnetic behavior should therefore be determined by a distribution of  $J$  couplings within the pairs. So a simple exchange coupled pairs model was proposed by Kahol et al. [150–152]:  $\chi = f_P \int \chi_{PAIR} P(J) dJ + (1 - f_P) N^2 \mu_B^2 / k_B T$ , where  $f_P$  is the fraction of total spins involved in pairs,  $P(J)$  is the distribution function for intrapair couplings,  $\chi_{PAIR} = (N^2 \mu_B^2 / k_B T) [3 + \exp(-2J/k_B T)]^{-1}$  is the magnetic susceptibility of a pair of spins,  $J$  varies from  $J_{min}$  to a maximum value  $J_0$ , and  $N$  is the number of spins in the disordered system. Assuming the distribution function  $P(J) = \text{constant}$  and  $J_0 \gg T$ , the above equation can be

simplified as  $\chi T = f_P \mu_B^2 [(2/3) \ln(3/4)(N/J_0)] T + N^2 \mu_B^2 (1 + f_P) / 3k_B$ , which exhibits a linear dependence of  $\chi T$  vs.  $T$ .

Although a lot of efforts have been focused on the magnetic properties of CPs through static magnetic measurements, electron paramagnetic resonance (EPR), or NMR spectroscopy, some of the results are still contradictory. For example, Jinder et al. [148] found that HCl-doped polyaniline shows a Pauli susceptibility, which is approximately linearly proportional to the degree of protonation. However, Raghunathan et al. [149] reported that the temperature-independent susceptibility of *p*-toluene sulfonic acid (PTSA) doped polyaniline decreases by one order of magnitude with increasing dopant concentration. The question is whether the temperature-independent susceptibility is a true Pauli susceptibility related with the density of states at the Fermi level. Some measurements on CP nanotubes/wires bring additional elements.

Long et al. [153] reported magnetic susceptibility measurements on conducting polyaniline and polypyrrole nanostructures with different dopant type and doping level as functions of temperature and magnetic field. It was found that the dc susceptibility  $\chi_{dc} = M_{dc}/B$  is dependent on the applied magnetic field  $B$  for some samples, which has been evidenced by the magnetic field dependence of magnetization ( $M_{dc}$  vs.  $B$  plot). For example, Fig. 16a and b show the magnetization  $M(B)$  as a function of magnetic field at high temperature (300 K) and low temperature (4 K or 5 K) for lightly doped and heavily doped PANI-NSA (naphthalene sulfonic acid) samples, respectively. For the lightly doped sample, paramagnetic behavior is evident both at 300 and 4 K, whereas the heavily doped sample shows diamagnetism at 300 K and paramagnetism at 5 K. However, for salicylic acid (SA) doped PANI samples, as shown in Fig. 16c, the lightly doped sample mainly shows diamagnetism at 300 K and very weak paramagnetic contribution only at weak magnetic field  $B < 1$  kOe. At  $T = 3$  K, a strong transition from paramagnetism to diamagnetism is observed in the  $M_{dc}$  vs.  $B$  plot. When the concentration is increased to  $[An]/[SA] = 1:1$ , the magnetic properties of PANI-SA becomes quite unusual. As shown in Fig. 16d, at  $T = 300$  K, the sample shows the signature of weak paramagnetism measured below  $B = 3.6$  kOe, which is dominated by a diamagnetic contribution at higher field. In particular, the sample only shows diamagnetism at  $T = 3$  K, no Curie-type paramagnetism is observed. Here we note, the above results can be repeated in other samples. For example, the magnetic field dependences of magnetization for *p*-toluene sulfonic acid doped polypyrrole (PPy-PTSA, [pyrrole]/[PTSA] = 1:0.3) nanostructures at 300 and 10 K are quite similar to those shown in Fig. 16c.

In addition, some unusual transitions were observed in the temperature dependence of susceptibility. For PANI-NSA nanostructures, the temperature-independent Pauli-like susceptibility decreases with the increase of doping level, as shown in Fig. 17a. In addition, paramagnetic susceptibility decreases gradually with decreasing temperature, as shown in Fig. 17b–d. These transitions suggest the coexistence of paramagnetic polarons and spinless bipolarons, with the possible formation of bipolarons (or polarons) with changes in doping level and temperature. According to the Shimoi-Abe model [157] taking

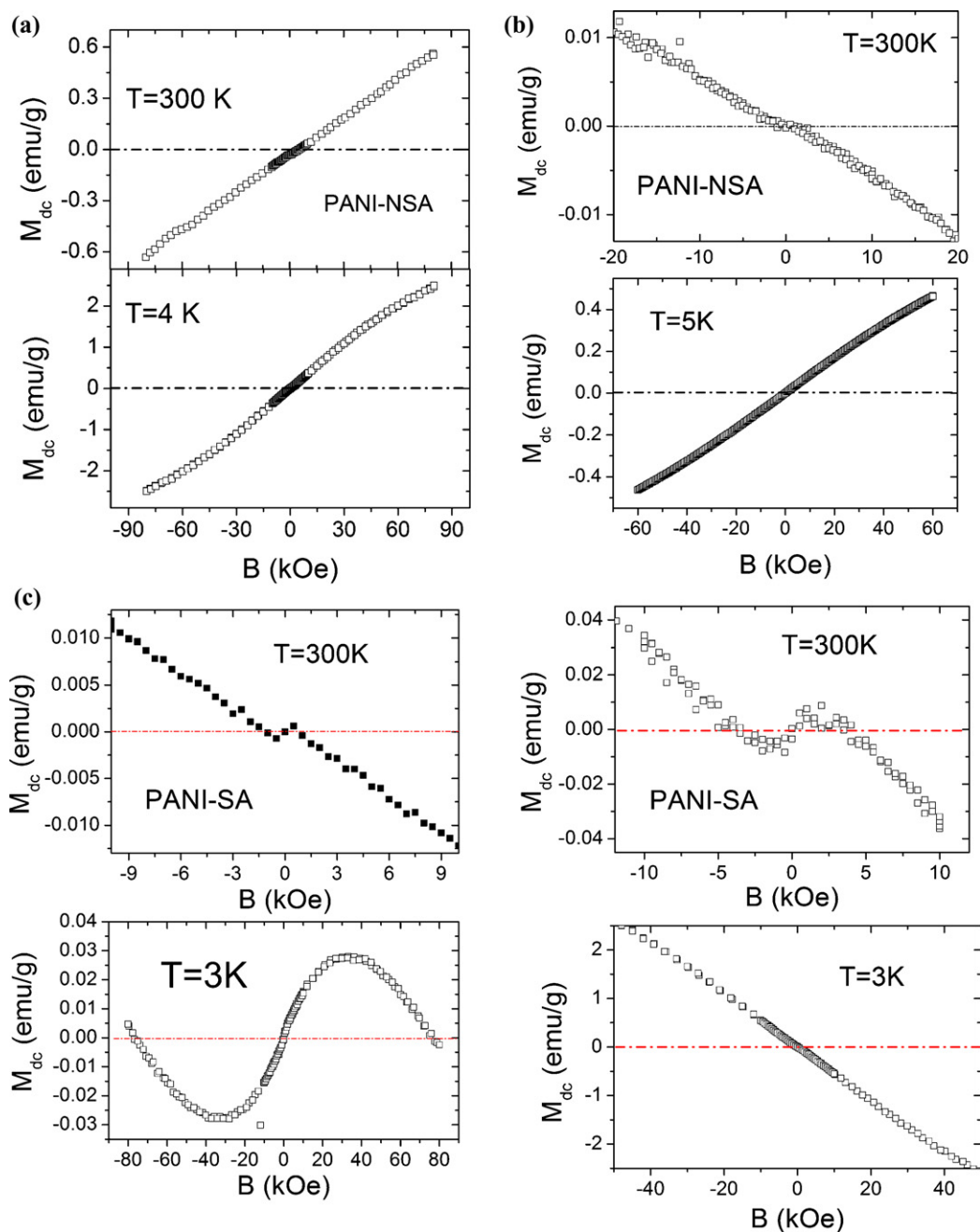


**Fig. 16.** Magnetic field dependences of magnetization for (a) lightly doped ( $[\text{aniline}]/[\text{NSA}] < 1:0.25$ ) and (b) heavily doped ( $[\text{aniline}]/[\text{NSA}] > 1:0.5$ ) PANI-NSA samples at room temperature and low temperature (4 or 5 K), and for salicylic acid doped polyaniline (PANI-SA) with doping level of  $[\text{aniline}]/[\text{SA}] = 1:0.1$  (c) and  $[\text{aniline}]/[\text{SA}] = 1:1$  (d) at 300 and 3 K [153]. Copyright 2006 American Chemical Society.

account of Coulomb effects on bipolarons and polarons, the polaron is the most stable configuration at low doping levels, and a doping-induced phase transition from a polaron lattice to a bipolaron lattice is possible because polarons are destabilized at high concentration of carriers. Furthermore, the doping level and dopant type may also strongly influence the relative stability of polarons and bipolarons by changing the microcrystalline structure during sample preparation (e.g., degree of conjugation,

degree of cross linking, interactions between charge carriers, counter-anions and other particles).

The above results indicate that the magnetic susceptibilities of doped polyaniline and polypyrrole nanostructures are strongly dependent on the doping level, dopant type, temperature, and extent of disorder, which result in a change of the relatively ratio (equilibrium) of localized spins, mobile spins, and spinless bipolarons. These results also suggest that we could not simply estimate the

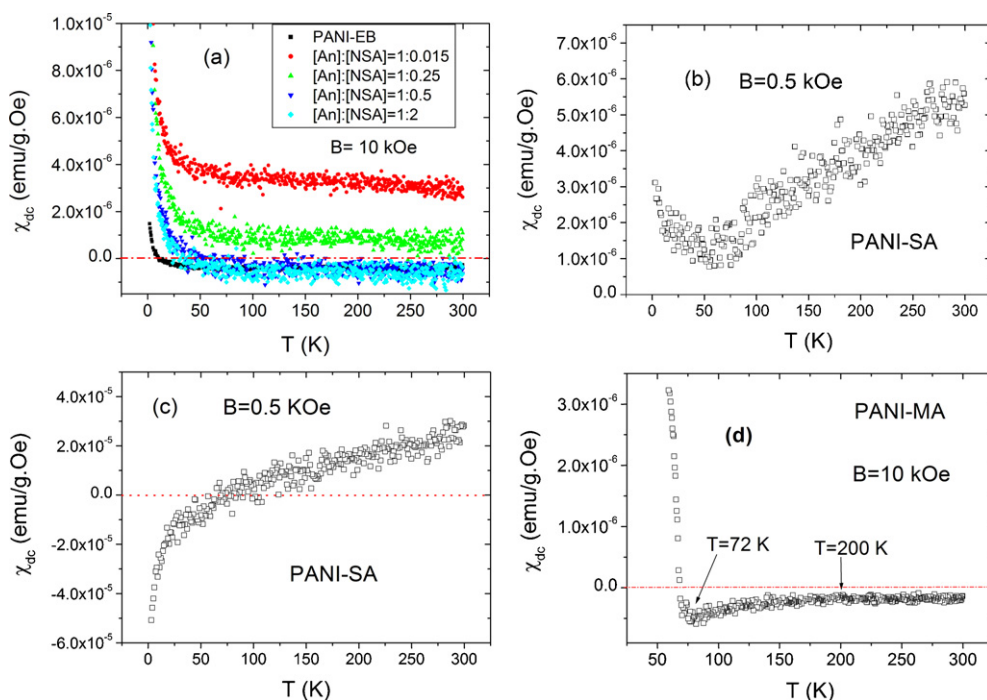


**Fig. 17.** Temperature dependences of dc magnetic susceptibility  $\chi_{dc}$  for different types of nanostructures: (a) naphthalene sulfonic acid doped polyaniline (PANI-NSA) with different molar ratio of [aniline]/[NSA] measured at magnetic field  $B = 0.5$  kOe, (b) lightly doped ([aniline]/[SA] = 1:0.1) and (c) heavily doped ([aniline]/[SA] = 1:1) PANI-SA sample measured at magnetic field  $B = 0.5$  kOe, and (d) molybdenic acid doped polyaniline (PANI-MA, [aniline]/[MA] = 1:1) measured at magnetic field  $B = 10$  kOe [153]. Copyright 2006 American Chemical Society.

density of states at the Fermi level through static magnetic susceptibility measurements ( $\chi_p = \mu_B^2 N(E_F)$ , where  $\mu_B$  is the Bohr magneton), because the temperature-independent susceptibility is dependent on the applied magnetic field [134,139] and cannot include the contribution of spinless bipolarons (which have a contribution to electrical conductivity). We note that the interpretation of the magnetic behavior of CPs is still controversial. For example, the concept of bands of ferromagnetic and antiferromagnetic correlated polarons and singlet ( $S=0$ ) and triplet ( $S=1$ ) bipolarons was proposed recently to explain both the ferromagnetic behavior and the magnetic field dependence [154,158]. So, systematic theoretical and experimental studies are still needed for this field of research [154,158,159].

### 3.3. Specific heat capacity of polyaniline nanotubes

As we know, the specific heat can be written as  $C_p(T) = \gamma T + \beta T^3$  for metals, where  $\gamma T$  and  $\beta T^3$  are the electronic and lattice contributions, respectively, to the specific heat. For CPs, only a few papers report the specific heats at low temperatures [151,152,160–167]. The temperature dependences (0.8–7 K) of the specific heats of pure polyacetylene and heavily doped metallic polyacetylene were firstly reported by Moses et al. [160]. Kahol et al. [162] reported the low temperature specific heat of polyaniline film and polyaniline-polymethylmethacrylate (PANI-PMMA) blends. It was found that the specific heat was represented at low temperatures (0.4–16 K) by  $C_p(T) = A + \gamma T + \beta T^3$  for the polyaniline film and by

$C_p(T) = \gamma T + \beta T^3$  for the PANI-PMMA blends. They calculated the corresponding density of states at the Fermi level according to the free-electron model. Gilani [163] studied the specific heats of highly conductive *p*-toluene sulfonate doped polypyrrole and metallic PF<sub>6</sub>-doped polypyrrole films in the temperature range of 0.6–12 K. It was found that at low temperature, a finite electronic contribution  $\gamma$  prevails in all samples. Namely, highly-doped polypyrrole behaves like a metal with finite density of states at Fermi level. These results indicate that the free-electron model is applicable to the metallic conjugated polymeric systems. However, the applicability of the free-electron model to CPs in the critical and insulating regimes of the metal-insulator transition is questionable, especially when temperature is below 10 K, because previous studies on dc conductivity (e.g., see Section 3.1), frequency-dependent conductivity, magnetic susceptibility (e.g., see Section 3.2) and thermoelectric power indicate that charge carriers in these non-metallic polymers strongly localized at low temperature due to disorder and/or electron-electron interactions [15,16].

Xu and Long et al. [164,165] studied the specific heat of polyaniline nanotubes prepared by template-free self-assembly method. Fig. 18a shows the specific heat of camphor sulfonic acid (CSA) doped polyaniline nanotubes ( $\sigma_{RT} \sim 6$  S/cm) between 1.8 and 45 K in the form of a  $C_p/T$  versus  $T^2$  plot. The inset shows the low temperature data (1.8–6.3 K). The linear fit passes through the origin, which indicates an electronic specific heat ( $\gamma T$ ) is not observed from the present data. The possible reason is that the polyaniline nanotubes are not metallic and charge carriers

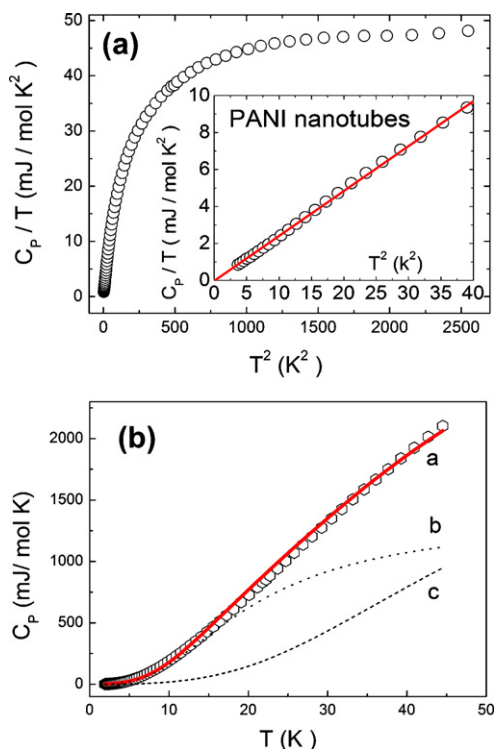


**Fig. 18.** (a) The specific heat of polyaniline nanotubes, plotted as  $C_p/T$  versus  $T^2$ . The inset shows the low temperature data (1.8–6.3 K). (b) The temperature dependence of the specific heat; curve *a* shows the fit to  $C_p(T) = D_g C_{cr}(T) + (1 - D_g) C_{am}(T)$ , curve *b* shows the contribution from amorphous regions and curve *c* shows the contribution from crystalline regions of the polymer nanotubes [165]. Copyright 2004 IOP Publishing Ltd.

ers are strongly localized to polymer chains. This result demonstrates that the free-electron model is not suitable for the present self-assembled polymer nanotubes. In view of the inhomogeneous disorder picture, it is proposed that the lattice specific heat of the polymer nanotubes can be expressed as a linear overlap of the heat capacities from the crystalline and amorphous regions [166]:

$$C_p(T) = D_g C_{cr}(T) + (1 - D_g) C_{am}(T) \quad (3)$$

$$C_{cr}(T) = 9\nu R \left( \frac{T}{\theta_D} \right)^3 \int_0^{\theta_D/T} \frac{x^4 \exp(x)}{[\exp(x) - 1]^2} dx \quad (4)$$

$$C_{am}(T) = 9\nu R \left( \frac{T}{\theta_D} \right)^3 \int_0^{\theta_{co}/T} \frac{x^4 \exp(x)}{[\exp(x) - 1]^2} dx + 9\nu R \left( \frac{T}{\theta_D} \right) Q \int_{\theta_{co}}^{\theta_M/T} \frac{x^2 \exp(x)}{[\exp(x) - 1]^2} dx \quad (5)$$

Here the parameter  $D_g$  expresses the corresponding crystallinity fraction. The contribution from the crystalline phase  $C_{cr}(T)$  has been evaluated by the usual Debye theory, and that from the amorphous phase  $C_{am}(T)$  has been analyzed in terms of a phonon-fraction model [167]:  $\nu$  is the number of atoms per formula unit,  $R$  is the molar gas constant,  $Q$  is a dimensionless constant,  $\theta_D$  is the Debye temperature,  $\theta_{co}$  and  $\theta_M$  are the crossover frequency

temperature and the maximal frequency temperature, respectively. Fig. 18b shows that the data can be well fitted using the above equation. The calculated Debye temperature  $\theta_D$  is 218.5 K. The obtained crystallinity fraction  $D_g$  is about 10–15%, which is small compared with the values reported for highly conductive polyaniline films ( $D_g$  is about 40–50%) [168]. This result is consistent with the inhomogeneous disorder picture of the polymer nanotubes/wires.

#### 3.4. Optical properties and optically-related properties: photoconductance, electrochromism and photothermal effect

Besides improved and tunable electrical properties, nanotubes/fibers of polyaniline, polypyrrole and PEDOT also show some interesting optical and optically-related properties [169–176]. For example, when PEDOT nanotubes are oxidized by applying a positive potential, the color of PEDOT turns from a deep blue (reduced state) to a transparent pale blue (oxidized state) [169,170]. In addition, it has been shown that PEDOT nanowires exhibit improved electroactivity and electrochromism by a comparative analysis between UV–Vis-near infrared spectra measured on PEDOT nanowires (diameter: 80 nm, 30 nm) and a thin film [171]. Particularly, template-synthesized PEDOT nanotubes have been demonstrated to be an excellent electrochromic material for electronic paper due to their facile fabrication, good color, mechanical stabilities, and ultrafast switching speeds. [169,170] Since the thin walls (10–20 nm) of PEDOT nanotubes render the diffusion distance of counter-ions extremely short, the switching speeds can be less than 10 ms, which are compatible with moving-image display technology. In recent years, photosensitivity and photoresponse of individual CP nanofibers have also been reported. For instance, a clear increase of conductance was observed when a polyaniline nanofiber was illuminated by a UV lamp, which can be explained as carrier generation in polyaniline nanofibers by UV illumination [172]. Wang et al. [173,174] observed similar results: the current of a bundle of polyaniline and polypyrrole nanowires under illumination by an incandescence lamp is enhanced by 4–6 times, and the devices exhibited clear photocurrent switching characteristics during switching on/off.

Another interesting phenomenon, a photothermal effect on CP nanofibers, was reported recently. Compared with bulk materials, nanofibers have a much larger efficient photothermal conversion and lower thermal conductivity, because the heat generated through photothermal processes will be confined within the individual nanofibers. It was found that a random network of polyaniline nanofibers under a camera flash irradiation was turned into a smooth and shiny film [175]. This flash welding technique (photothermal effect) can be used to fabricate asymmetric nanofiber films, to melt polymer/polymer nanocomposites rapidly and to photo-pattern polymer nanofiber films [176,177].

The optical properties of CP nanostructures can also be modified by using a functional dopant method. For example, azobenzene sulfuric acid doped polyaniline nanotubes

synthesized by template-free method show *trans*–*cis* photoisomerization upon irradiation with UV light [178]. Zhang et al. [62] reported polyaniline hollow microspheres with a strong fluorescence and a high conductivity ( $\sim 10^{-1}$  S/cm), which were prepared by the template-free method in the presence of Rhodamine B (RhB) as a fluorescent material.

### 3.5. Mechanical properties

Recently, the mechanical properties of a single nanofiber/tube have drawn much attention [for a review, see Ref. [179]]. Elastic modulus of individual nanotubes and nanofibers of conjugated polymers such as polypyrrole, polyacetylene and PEDOT were measured using atomic force microscopy. [97,180–183] Cuenot et al. [180] first reported the elastic tensile modulus of template-synthesized polypyrrole nanotubes with an outer diameter ranging between 30 and 250 nm, deduced from force-curve measurements or resonance-frequency measurements. It was found that the elastic modulus strongly increased when the thickness of the polypyrrole nanotubes wall or its outer diameter decreased: the elastic modulus varies between 1.2 and 3.2 GPa for tubes with outer diameter larger than 100 nm and wall thickness higher than 20 nm (as a set of comparison, Park et al. found about 1 GPa for a polypyrrole nanotube with an outer diameter of 120 nm [97]). With decreasing thickness or outer diameter, the nanotube's elastic modulus strongly increases and can reach a value close to 60 GPa for a wall thickness of 6.5 nm and an outer diameter of about 35 nm. Similar size-dependent mechanical behavior has been also observed in other single polymer nanofibers [179,184–186]. The observed behavior for the elastic modulus is very similar to that previously observed for the electrical conductivity. That suggests that the structural improvement induced by the template synthesis for the smaller nanotubes diameters could be responsible for the mechanical behavior. However, both theoretical models and experimental studies (e.g., measuring apparent elastic modulus [182]) have shown recently that the increase of elastic modulus for lower diameters comes essentially from surface effects [182,184,185,189]. Precisely, when the surface-volume ratio increases, an additional term including the surface effects (mainly surface tension) may become predominant [182]. Here it should be noted that similar size-dependent mechanical behavior has been also observed in inorganic nanowires such as CuO [187], silicon [188], silver and lead [189] nanowires. Of course, the structural improvement as induced by the template synthesis for the (super)molecular structure cannot be considered for these inorganic systems.

### 3.6. Microwave absorbing property

CPs as new microwave absorbing materials have been explored due to their lower density and their easy processability. In general, traditional films or pellets of doped polyaniline and polypyrrole only exhibit an electrical loss in the microwave frequency (e.g.,  $f = 1$ –18 GHz) [190–192]. However, Wan et al. [193] found that PANI-NSA and PANI-NSA/glucose micro/nano-tubes prepared by the

template-free method show an excellent electro-magnetic loss. For comparison, the dopant NSA, aniline salt formed with NSA and granular PANI-NSA exhibited only weak or no magnetic loss (Figs. 6 and 7 of Ref. [193]). Obviously, the tubular morphology contributed to the strong magnetic loss observed in the polymer microtubes at  $f = 10$ –18 GHz. Namely, it may arise from an enhanced chain ordering (or partial order of the polaron as charge carrier) induced by the tubular morphology [193]. In addition, Liu et al. [194] studied the electromagnetic wave absorbing property of polyaniline/polystyrene composite. It was found that the doped polyaniline with fiber-like morphology has better electromagnetic wave absorbing property than that of polyaniline with particle-like morphology. The frequency breadth of the reflectivity below  $-10$  dB is 6 GHz (11.6–17.6 GHz) by optimizing the electromagnetic parameters of the micro/nano-composite. The above results indicate that nanotubes/fibers of CPs can be used as high absorption, wide frequency and lightweight microwave absorbent.

## 4. Applications of conducting polymer nanotubes and nanofibers

### 4.1. Chemical, optical and bio-sensors

Since the electrical and optical properties of CPs can be reversible changed by a doping/dedoping process, CP nanostructures have been widely explored as chemical sensors, optical sensors and biosensors due to greater exposure area than the conventional bulk polymers. Previous studies demonstrate that the gas (HCl, NH<sub>3</sub>, NO, H<sub>2</sub>S, ethanol, liquefied petroleum gas [40], etc.) sensors based on polyaniline or PEDOT [195] nanofibers usually show a higher sensitivity and shorter response time because of higher surface areas [45,196–205]. For example, it was found that the response times of the polyaniline nanofiber sensors exposed to chloroform, toluene and triethylamine were about a factor of 2 faster, with the current variations up to 4 times larger than those of the bulk polyaniline sensors [198].

NH<sub>3</sub>, NO, and pH sensors based on individual polyaniline, PEDOT, polypyrrole nanofibers/wires have also been reported [76,82,83,206–210]. For instance, single polyaniline nanowire chemical sensors showed a rapid and reversible resistance change upon exposure to NH<sub>3</sub> gas at concentrations as low as 0.5 ppm [76]. The response times (on the order of 10 s to a few minutes) of nanowire sensors with various diameters correspond to radius-dependent differences in the diffusion time of NH<sub>3</sub> gas into the wires. NO gas sensors based on single and multiple PEDOT nanowires were also reported by Lu et al. [207]. The responses to NO were highly linear, reproducible and reliable with a minimal concentration of NO of 10 ppm.

Pringsheim et al. reported that fluorescent beads coated with polyaniline can be used as a novel optical pH sensor [211]. The fluorescence emitted by dye-doped polymer nanobeads is modulated by a thin conductive polyaniline coating, whose visible-light absorption varies with pH at values around seven. Gu et al. [212,213] demonstrated a single waveguiding polyaniline/polystyrene nanowire

for highly selective optical detection of gas mixtures (sensing with a response time of 30 ms for humidity; detection down to subparts-per-million level for NO<sub>2</sub> and NH<sub>3</sub>). In addition, the photosensitivity and photoresponse of a bundle of polyaniline nanowires were also investigated by Wang et al. [173,174], which showed that the photocurrent enhanced by 4–5 times under irradiation of an incandescence lamp (12 V, 10 W). These results indicate that CP nanofibers might be useful in the fabrication of photosensor and photoswitch nanodevices. In addition, Zhu et al. [8,9,224,225] reported a pH sensor of polyaniline-perfluorosebacic acid (PFSEA)-coated fabric guided by reversible switching wettability through a PFSEA doping/NH<sub>3</sub> dedoping process. It was found that the CP nanostructure-based sensors show a fast response, stability, and good reproducibility by changing wettabilities from superhydrophobic (doping) to superhydrophilic (dedoping).

Biosensors based on CP nanotubes/wires were also explored intensively in recent years [214–223]. For instance, Zhang et al. [215] reported poly(methyl vinyl ether-alt-maleic acid) doped polyaniline nanotubes for oligonucleotide sensors. Peng et al. [216] reported a functionalized polythiophene as an active substrate for a label-free electrochemical geno-sensor. In addition, Langer et al. [217] reported a bacteria nanobiodetector based on a limited number of polyaniline nanofibers. The device works like an “ON-OFF” switch with nearly linear response above a threshold number of cells in the suspension examined, and may be useful in bio-alarm systems, environmental monitoring and medical applications.

#### 4.2. Field effect transistors and diodes

Field-effect transistors based on individual CP nanofibers have been reported extensively [74,75,226–228]. Pinto et al. [74] reported an electrospun polyaniline/polyethylene oxide nanofiber field-effect transistor. Liu et al. [75] reported a single nanofiber field-effect transistor from electrospun poly(3-hexylthiophene). The transistor exhibited a hole field-effect mobility of 0.03 cm<sup>2</sup>/V s in the saturation regime, and a current on/off ratio of 10<sup>3</sup> in the accumulation mode. An ultra-short poly(3-hexylthiophene) field effect transistor with effective channel length down to 5–6 nm and width ~2 nm was also reported by Qi et al. [226]. In addition, Alam et al. [227] reported electrolyte-gated transistors based on conducting polyaniline, polypyrrole and PEDOT nanowire junction arrays. In the presence of a positive gate bias, the polyaniline nanowire-based transistors exhibit a large on/off current ratio of 978, which can vary according to the acidity of the gate medium. Lee et al. [228] also reported electrolyte-gated conducting polyaniline nanowire field-effect transistors.

Besides nanofiber field effect transistors, nanostructured polymer/semiconductor (metal) diodes were also reported. Guo et al. [26,27] reported an organic/inorganic p–n junction nanowire consisting of polypyrrole and CdS fabricated using an Al<sub>2</sub>O<sub>3</sub> template, which displays a strong photo-dependent rectifying effect. It was also reported that single Au-polypyrrole-Cd-Au nanorods exhibit diode behavior

with rectifying ratio ~200 at ±0.6 V at room temperature [229]. Pinto et al. [230,231] reported a Schottky diode using an n-doped Si/SiO<sub>2</sub> substrate and an electrospun fully doped polyaniline nanofiber. Liu et al. [102] demonstrated that Au/template-synthesized polypyrrole nanofiber devices show rectifying behavior, and might be used as nano-rectifiers.

#### 4.3. Polymer light-emitting diodes, field-emission and electrochromic displays

Well-aligned polyaniline, polypyrrole, and PEDOT nanofibers/tubes have also been explored for polymer light-emitting diodes (PLEDs) [232–235], field emission [24,236–238] and electrochromic [169,170,239–241] displays. For example, micrometer- and nanometer-sized polymeric light-emitting diodes based on hard template-synthesized PEDOT nanowires were first reported by Granström et al. [232]. Boroumand et al. [234] fabricated arrays of nanoscale conjugated-polymer light-emitting diodes, each of which has a hole-injecting contact limited to 100 nm in diameter. Concerning field-emission applications, it was found that polyaniline nanofibers within hard template membrane showed stable field emission behavior with low threshold voltage of 5–6 V/μm and high emission current density of 5 mA/cm<sup>2</sup> [236]. For field emission cell of template-synthesized PEDOT nanowires [237,238], the turn-on field was 3.5–4 V/μm, the current density was 0.1 mA/cm<sup>2</sup>, and the field enhancement factor of nanotips was about 1200, which is comparable to those of carbon nanotubes. These results suggest that the polyaniline, PEDOT, and polypyrrole nanofibers/tubes can be used as nanotips for field emission displays. However, the stability of organics into such high-field and the resulting increase in temperature has to be addressed. In addition, due to the ability to change color under an applied potential, CP nanostructures have been investigated as the active layer in electrochromic devices [169,170,239–241]. For instance, Cho et al. [169] demonstrated a fast color-switching electrochromic device based on nanotubular PEDOT. An electrochromic device from nanostructured PEDOT grown on vertical Si nanowires was also reported [241].

#### 4.4. Energy storage

Electrochemical studies on CP nanostructures have demonstrated that they usually have higher specific capacitance values and can be beneficial in the development of the next-generation energy storage devices [242–247]. Zhang et al. reported that PANI nanofibers showed higher capacitance values and more symmetrical charge/discharge cycles due to their increased available surface area [32,244]. The highly dense arrays of ordered and aligned nanorods of polyaniline with 10 nm diameter were found to exhibit excellent electrochemical properties with an electrochemical capacitance value of 3407 F/g [245]. Template-synthesized PEDOT nanotubes also show high power capability: the specific capacitance value is 132 F/g, and the device retains a high energy density (5.6 Wh/kg) at a high power, which can be attributed to

the fast charge/discharge of nanotubular structures: hollow nanotubes allow counter-ions to readily penetrate into the polymer and access their internal surfaces [247]. It was also reported that  $\text{MnO}_2$ /PEDOT coaxial nanowires prepared by a one-step coelectrodeposition in a porous alumina template show very high specific capacitances even at high current densities. The excellent electrochemical and mechanical properties indicate that the coaxial nanowires may lead to new types of nanomaterials in electrochemical energy storage devices [30].

Fuel and photovoltaic cells are also concerned by polymeric nanofibers. Kim et al. [248] reported template-synthesized polypyrrole nanowire-based enzymatic biofuel cells. It was found that the nanowire-type biofuel cell exhibited a higher power density than the film-type biofuel cell by two orders of magnitude. Particularly, single polypyrrole-CdS nanowire photovoltaic cells were reported recently [26,27]. We note that conjugated-polymer-based photovoltaic elements (plastic solar cells) have been extensively reported, for a good review see Ref. [249].

#### 4.5. Drug release and protein purification

Drug delivery devices have flourished during the last few decades and are extensively used in various kinds of treatments. In this context, conducting polymer-based

devices have been investigated to examine how they can serve as electrically controlled drug delivery devices inside the body. One major challenge is to develop a drug delivery system that allows strict control of the ON/OFF state. In addition, such a device must be able to deliver the drug of interest at doses that are required to obtain the therapeutic effect. Abidian et al. [41] reported an on-demand drug realizing system based on PEDOT nanotubes, as shown in Fig. 19. In this approach, poly(lactide-co-glycolide)/dexamethasone fibers were formed and grown using electrospinning onto a supporting electrode, and PEDOT was thereafter electrochemically grown along the surface of the fibers to form PEDOT nanotubes. The release characteristics of dexamethasone were studied while the carrying electrode was biased at different voltages. The cumulative mass release of dexamethasone was found to increase dramatically as short voltage pulses were applied to the electrode hosting the PEDOT/poly(lactide-co-glycolide)/dexamethasone fibers. The electrically controlled release in this case is tentatively attributed to two parallel effects. First, as the oxidation state of PEDOT cladding layer is switched, a contraction force on the poly(lactide-co-glycolide)/dexamethasone fiber core is induced. This force squeezes the core of the fiber, affecting the transport as well as the kinetics of the drug molecule. More important, it is expected that the PEDOT-cladding may crack during a switch cycle. This may result in addi-

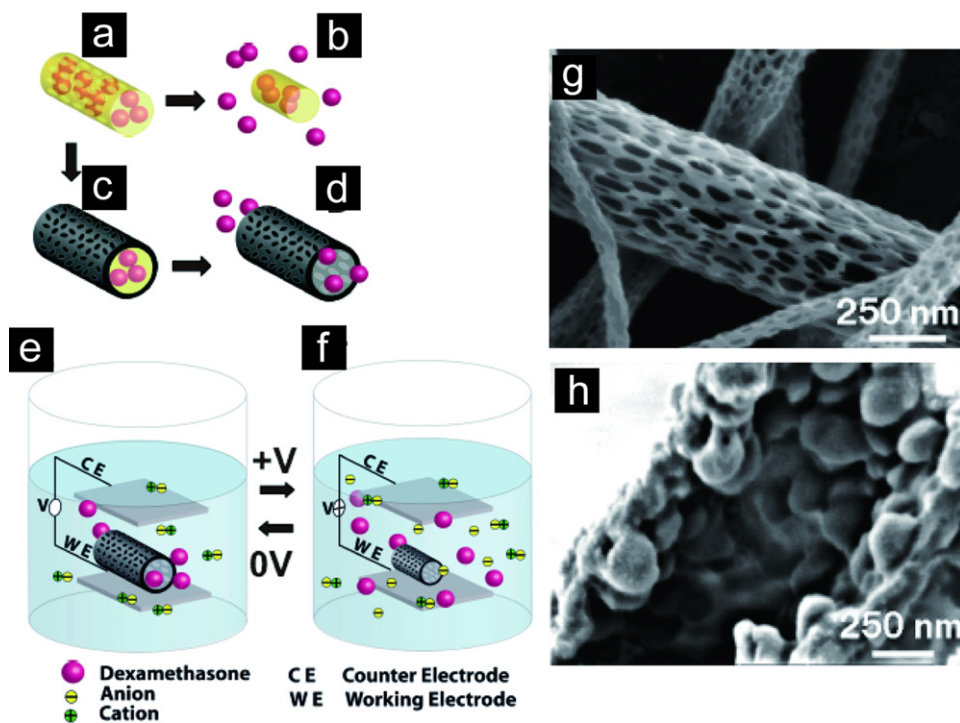


**Fig. 19.** Schematic illustration of the controlled release of dexamethasone: (a) dexamethasone-loaded electrospun poly(lactide-co-glycolide) (PLGA), (b) hydrolytic degradation of PLGA fibers leading to release of the drug, and (c) electrochemical deposition of PEDOT around the dexamethasone-loaded electrospun PLGA fiber slows down the release of dexamethasone (d). (e) PEDOT nanotubes in a neutral electrical condition. (f) External electrical stimulation controls the release of dexamethasone from the PEDOT nanotubes due to contraction or expansion of the PEDOT. By applying a positive voltage, electrons are injected into the chains and positive charges in the polymer chains are compensated. To maintain overall charge neutrality, counterions are expelled towards the solution and the nanotubes contract. This shrinkage causes the drugs to come out of the ends of tubes. SEM images of (g) PLGA nanoscale fibers and (h) a single PEDOT nanotube which was polymerized around a PLGA nanoscale fiber, followed by dissolution of the PLGA core fiber [adapted from Ref. [41]]. Copyright 2006 Wiley-VCH Verlag GmbH & Co. KGaA, Weinheim.

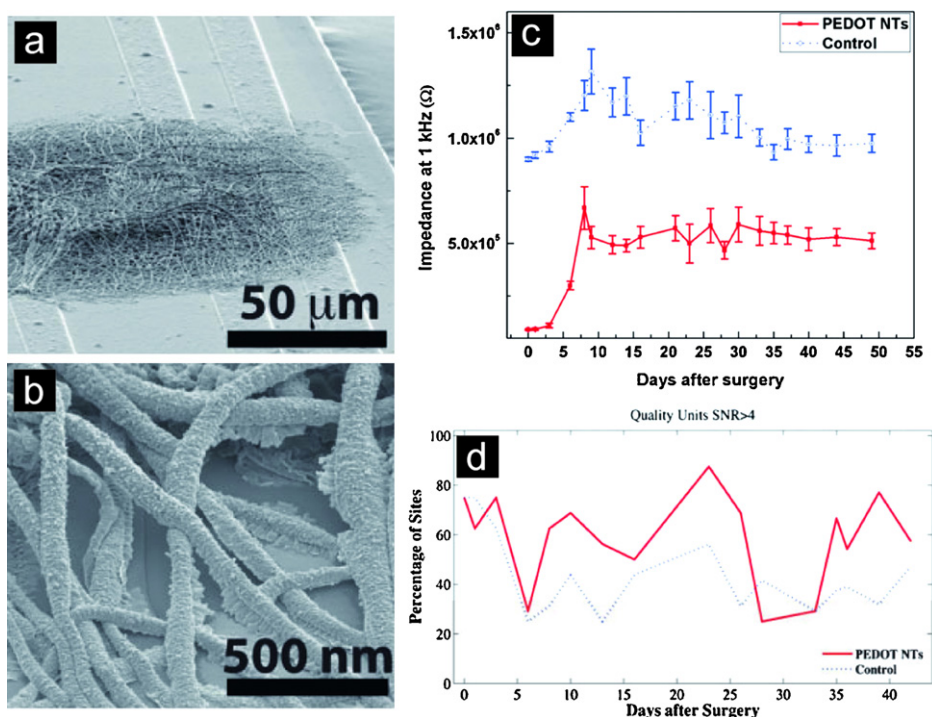


**Fig. 20.** SEM images of PEDOT nanotubes from lower (a) to higher magnification (b) on the surface of a single microelectrode site. (c) The in vivo impedance spectroscopy in a rat model during seven weeks post implantation. (d) Neural recording activity of animal during seven weeks post implantation of this article for more clarification [adapted from Ref. [43]]. Copyright 2009 Wiley-VCH Verlag GmbH & Co. KGaA, Weinheim.

tional pathways for the dexamethasone drug to escape the poly(lactide-co-glycolide) core host via nano-cracks through the PEDOT nanotubes.

In addition, Shi et al. [250] reported chemically modified poly(1-(2-carboxyethyl)pyrrole) microtubes could be used as an affinity matrix for protein purification. Elution of the protein showed that the desorption ratio was up to 99.5%. Furthermore, it is found that the adsorption–desorption cycle was repeated 10 times using the same microtubes without significant loss in the hemoglobin adsorption capacity.

#### 4.6. Neural interfaces

Abidian et al. [251] have demonstrated a fabrication method for the growth of conducting polymer nanofibers within a hydrogel scaffold coated on neural microelectrodes (Fig. 20a and b). In this paper, Abidian et al. describe the design and characterization of a multifunctional, hybrid nanostructured interface for neural microelectrodes that is soft, low impedance, has high charge density, and is capable of controlled drug release [41]. The design includes: (i) biodegradable electrospun nanofibers for the controlled release of drugs and to provide a scaffold for the formation of conducting polymer nanotubes and (ii) hydrogel layers for the sustained release of drugs, and to provide a scaffold for the formation of nanostructured cloud-like conducting polymer. The hydrogel coatings provide a mechanical buffer layer between the hard silicon-based probe and the soft brain tissue, a scaffold for growing the conducting poly-

mer within the hydrogel matrix, and a diffusion barrier for controlling drug release. They have also compared electrical properties of different combinations of conducting polymer nanofibers and nanotubes within the hydrogel in terms of impedance spectroscopy and capacity of charge density.

They have shown that the minimum impedance occurred in the case of combination of PEDOT nanotubes and PEDOT within the hydrogel. The impedance decreased significantly at 1 kHz from 783 kΩ (bare gold) to 2.5 kΩ (PEDOT nanotubes + hydrogel + PEDOT) (Fig. 20) [251]. Abidian et al. also demonstrated that the charge density increased significantly, about 2 orders of magnitude, from 1.28 mC/cm<sup>2</sup> to 223.8 mC/cm<sup>2</sup> in the case of PEDOT nanotubes + hydrogel + PEDOT [251]. They also demonstrated that electrodes modified with PEDOT nanotubes registered high quality unit activity (signal-to-noise ratio, SNR > 4, as shown in Fig. 20d) on 30% more sites than uncoated controls, primarily as a result of reduced noise. They also showed that sites modified with PEDOT nanotubes had significantly less low frequency artifact in local field potential recordings. The Nyquist plots of in vivo electrochemical impedance spectroscopy measurements revealed that the PEDOT nanotubes may be used as a novel method for biosensing to indicate the transition between acute and chronic responses in brain tissue [43,251]. In addition, it has been shown that polypyrrole and PEDOT nanotubes can adhere better to the surface of electrodes in comparison with their film counterparts [44].

#### 4.7. Actuators and other applications

Potential applications of CP bulk films and nanostructures on actuators or artificial muscles have also drawn much attention [177,252–258]. For example, Okamoto et al. [253] reported an actuator based on doping/undoping-induced volume change in anisotropic polypyrrole film. Otero and Cortes [254] reported the movement of an all polymeric triple-layer artificial muscle based on polypyrrole. Recently, it was reported that flash-welded polyaniline nanofiber actuators demonstrate unprecedented reversible, rapid actuation upon doping [177]. An asymmetric nanofiber film with a thin dense layer on top of a thick porous nanofibrillar layer is formed by an intense flash of light; the layer can curl more than 72° on exposure to camphor sulfonic acid [177]. Actuation response (or reversible volume changes with electrode potential) in polypyrrole and polyaniline nanostructures were also investigated by electrochemical AFM (atomic force microscopy) [255,258].

Besides all the potential applications reported above, some other applications of CP-based nanofibers have been investigated. For instance, Yang et al. [259] reported that polyaniline nanofibers have better corrosion protection for mild steel than conventional aggregated polyaniline. Polyaniline microtubes/nanofibers [193,194] and polyaniline-multiwalled carbon nanotubes nanocomposites [260] may be used as microwave absorbers and electromagnetic interference shielding materials. It was also reported that conducting polyaniline nanofibers were used as nanofillers to improve the electrical properties of a ferroelectric copolymer [261]. In addition, polyaniline nanofibers decorated with gold nanoparticles exhibited very interesting bi-stable electrical behavior, and can be switched electrically between two states, which may be used in the fabrication of plastic digital nonvolatile memory device [262].

### 5. Summary and outlook

During the last 20 years, significant progress has been made in synthesis, morphological and structural characterizations, physical and chemical properties of CP nanofibers and nanotubes. This article is a brief review on these fast growing research areas in order to understand the specific behavior and potential applications of one-dimensional CP nanostructures in comparison to their bulk materials.

To date, a variety of approaches have been employed to synthesize and fabricate CP nanostructures. However, facile, efficient, and large-scale synthesis of the nanostructures of CPs with uniform, non-disperse, and well-desire morphology and size, even oriented nanostructure arrays, is still desired. In addition, the currently reported polymer nanostructures produced by these methods are usually amorphous or partially crystalline. In some strategies, the polymeric structure can be improved in comparison to the bulk case, but fabrication of highly crystalline and metallic polymer nanotubes and nanofibers is still a challenge.

CP nanotubes and nanofibers have displayed an impressive applicative potential from energy harvesting and bio-/chemical sensing to electronic devices and drug deliv-

ery. However, due to the complicated microstructures of CPs, there are still problems to fulfill their applications in nanoscale devices, such as the reproducibility and/or controllability of individual polymer nanotubes/wires, stability of the doping level and improving processability of CP nanostructures. Previous studies of individual nanodevices (diodes and transistors) based on isolated tubes/fibers represent only an initial step towards nanoelectronic circuits. It remains a great challenge to assemble or fabricate integrated functional circuits from single devices. Furthermore, synthesizing CP nanostructures with improved electrical conductivity and/or mobility will enhance the performance of the devices and many of the applications discussed. Finally, it is worth noting that CP-based hybrid nanostructures [26–31,204,260–270] offer a very broad and promising field of research, not only to enhance the above-mentioned properties and to address the corresponding challenges for applications, but also to achieve multifunctional nano-systems and then, to open new perspectives.

### Acknowledgements

This work was financially supported by the National Natural Science Foundation of China (Grant Nos.: 11074138, 10910101081, 10604038, 10374107 and 50825206) and the Program for New Century Excellent Talents in University of China (Grant No.: NCET-07-0472). Part of this work has been supported by the Communauté urbaine de Nantes, France. The authors are also grateful to Dr. Stephane Cuenot at the Institut des Matériaux Jean Rouxel for revising Section 3.5: Mechanical Properties.

### References

- [1] Kuchibhatle SVNT, Karakoti AS, Bera D, Seal S. One dimensional nanostructured materials. *Prog Mater Sci* 2007;52:699–913.
- [2] (a) Lupu N. Nanowires science and technology. Croatia: InTech, <http://sciendo.com/books/show/title/nanowires-science-and-technology>; 2010;  
(b) Li RJ, Hu WP, Liu YQ, Zhu DB. Micro- and nanocrystals of organic semiconductors. *Acc Chem Res* 2010;43:529–40.
- [3] Xia YN, Yang PD, Sun YG, Wu YY, Mayers B, Gates B, Yin YD, Kim F, Yan YQ. One-dimensional nanostructures: synthesis, characterization, and applications. *Adv Mater* 2003;15:353–89.
- [4] Hamed M, Forchheimer R, Inganös O. Towards woven logic from organic electronic fibres. *Nat Mater* 2007;6:357–62.
- [5] Akkerman HB, Blom PWM, de Leeuw DM, de Boer B. Towards molecular electronics with large-area molecular junctions. *Nature* 2006;441:69–72.
- [6] (a) Tran HD, Li D, Kaner RB. One-dimensional conducting polymer nanostructures: bulk synthesis and applications. *Adv Mater* 2009;21:1487–99;  
(b) Lu XF, Zhang WJ, Wang C, Wen TC, Wei Y. One-dimensional conducting polymer nanocomposites: synthesis, properties and applications. *Prog Polym Sci* 2010;36:671–712.
- [7] Li C, Bai H, Shi GQ. Conducting polymer nanomaterials: electrosynthesis and applications. *Chem Soc Rev* 2009;38:2397–409.
- [8] (a) Wan MX. Some issues related to polyaniline micro/nanostructures. *Macromol Rapid Commun* 2009;30:963–75;  
(b) Wan MX. Conducting polymers with micro or nanometer structure. Berlin, Heidelberg: Tsinghua University Press and Springer; 2008.
- [9] (a) Stejskal J, Sapurina I, Trchová M. Polyaniline nanostructures and the role of aniline oligomers in their formation. *Prog Polym Sci* 2010;35:1420–81;  
(b) Laslau C, Zujovic Z, Travas-Sejdic J. Theories of polyaniline nanostructure self-assembly: Towards an expanded, comprehensive Multi-Layer Theory (MLT). *Prog Polym Sci* 2010;35:1403–19.

- [10] MacDiarmid AG. Synthetic metals: a novel role for organic polymers. *Angew Chem Int Edit* 2001;40:2581–90.
- [11] (a) Heeger AJ. Semiconducting and metallic polymers: the fourth generation of polymeric materials. *Synth Met* 2001;125:23–42; (b) Heeger AJ. Semiconducting polymers: the third generation. *Chem Soc Rev* 2010;39:2354–71.
- [12] Zhang DH, Wang YY. Synthesis and applications of one-dimensional nano-structured polyaniline: an overview. *Mat Sci Eng B-Solid* 2006;134:9–19.
- [13] Jang J. Conducting polymer nanomaterials and their applications. *Adv Polym Sci* 2006;199:189–259.
- [14] Aleshin AN. Polymer nanofibers and nanotubes: charge transport and device applications. *Adv Mater* 2006;18:17–27.
- [15] Skotheim TA, Elsenbaumer RL, Reynolds JR. Handbook of conducting polymers. 2nd ed. New York: Marcel Dekker; 1998.
- [16] Skotheim TA, Reynolds JR. Handbook of conducting polymers. 3rd ed. Boca Raton: CRC Press; 2007.
- [17] Martin CR. Nanomaterials: a membrane-based synthetic approach. *Science* 1994;266:1961–6.
- [18] Martin CR. Template synthesis of electronically conductive polymer nanostructures. *Acc Chem Res* 1995;28:61–8.
- [19] Granström M, Inganäs O. Electrically conductive polymer fibres with mesoscopic diameters: 1. Studies of structure and electrical properties. *Polymer* 1995;36:2867–72.
- [20] Cai ZH, Lei JT, Liang WB, Menon V, Martin CR. Molecular and super-molecular origins of enhanced electronic conductivity in template-synthesized polyheterocyclic fibrils. 1. Supermolecular effects. *Chem Mater* 1991;3:960–7.
- [21] Duchet J, Legras R, Demoustier-Champagne S. Chemical synthesis of polypyrrole: structure-properties relationship. *Synth Met* 1998;98:113–22.
- [22] Duval JL, Rétho P, Fernandez V, Louarn G, Molinié P, Chauvet O. Effects of the confined synthesis on conjugated polymer transport properties. *J Phys Chem B* 2004;108:18552–6.
- [23] Mativetsky JM, Datars WR. Morphology and electrical properties of template-synthesized polypyrrole nanocylinders. *Physica B* 2002;324:191–204.
- [24] Kim BH, Park DH, Joo J, Yu SG, Lee SH. Synthesis, characteristics, and field emission of doped and de-doped polypyrrole, polyaniline, poly(3,4-ethylenedioxy-thiophene) nanotubes and nanowires. *Synth Met* 2005;150:279–84.
- [25] Massuyeau F, Duval JL, Athalin H, Lorcay JM, Lefrant S, Wéry J, Faulques E. Elaboration of conjugated polymer nanowires and nanotubes for tunable photoluminescence properties. *Nanotechnology* 2009;20, 155701/1–8.
- [26] Guo YB, Tang QX, Liu HB, Zhang YJ, Li YL, Hu WP, Wang S, Zhu DB. Light-controlled organic/inorganic p-n junction nanowires. *J Am Chem Soc* 2008;130:9198–9.
- [27] Guo YB, Zhang YJ, Liu HB, Lai SW, Li YL, Li YJ, Hu WP, Wang S, Che CM, Zhu DB. Assembled organic/inorganic p-n junction interface and photovoltaic cell on a single nanowire. *J Phys Chem Lett* 2010;1:327–30.
- [28] Gence L, Faniel S, Gustin C, Melinte S, Bayot V, Callegari V, Reynes O, Demoustier-Champagne S. Structural and electrical characterization of hybrid metal-polypyrrole nanowires. *Phys Rev B* 2007;76, 115415/1–8.
- [29] Callegari V, Gence L, Melinte S, Demoustier-Champagne S. Electrochemically template-grown multi-segmented gold-conducting polymer nanowires with tunable electronic behavior. *Chem Mater* 2009;21:4241–7.
- [30] Liu R, Lee SB. MnO<sub>2</sub>/poly(3,4-ethylenedioxythiophene) coaxial nanowires by one-step coelectrodeposition for electrochemical energy storage. *J Am Chem Soc* 2008;130:2942–3.
- [31] Lorcay JM, Massuyeau F, Moreau P, Chauvet O, Faulques E, Wéry J, Duval JL. Coaxial nickel/poly(p-phenylene vinylene) nanowires as luminescent building blocks manipulated magnetically. *Nanotechnology* 2009;20, 405601/1–7.
- [32] Zhang XY, Goux WJ, Manohar SK. Synthesis of polyaniline nanofibers by “nanofiber seeding”. *J Am Chem Soc* 2004;126:4502–3.
- [33] Zhang XY, Manohar SK. Bulk synthesis of polypyrrole nanofibers by a seeding approach. *J Am Chem Soc* 2004;126:12714–5.
- [34] Zhang XY, Manohar SK. Narrow pore-diameter polypyrrole nanotubes. *J Am Chem Soc* 2005;127:14156–7.
- [35] Pan LJ, Pu L, Shi Y, Song SY, Xu Z, Zhang R, Zheng YD. Synthesis of polyaniline nanotubes with a reactive template of manganese oxide. *Adv Mater* 2007;19:461–4.
- [36] Li X, Tian SJ, Ping Y, Kim DH, Knoll W. One-step route to the fabrication of highly porous polyaniline nanofiber films by using PS-b-PVP diblock copolymers as templates. *Langmuir* 2005;21:9393–7.
- [37] Nickels P, Dittmer WU, Beyer S, Kottaus JP, Simmel FC. Polyaniline nanowires synthesis template by DNA. *Nanotechnology* 2004;15:1524–9.
- [38] Houlton A, Pike AR, Galindo MA, Horrocks BR. DNA-based routes to semiconducting nanomaterials. *Chem Commun* 2009:1797–806.
- [39] Li X, Wan MX, Li XN, Zhao GL. The role of DNA in PANI-DNA hybrid: template and dopant. *Polymer* 2009;50:4529–34.
- [40] Rong JH, Oberbeck F, Wang XN, Li XD, Oxsher J, Niu ZW, Wang Q. Tobacco mosaic virus templated synthesis of one dimensional inorganic-polymer hybrid fibres. *J Mater Chem* 2009;19:2841–5.
- [41] Abidian MR, Kim DH, Martin DC. Conducting-polymer nanotubes for controlled drug release. *Adv Mater* 2006;18:405–9.
- [42] Abidian MR, Martin DC. Experimental and theoretical characterization of implantable neural microelectrodes modified with conducting polymer nanotubes. *Biomaterials* 2008;29:1273–83.
- [43] Abidian MR, Ludwig KA, Marzullo TC, Martin DC, Kipke DR. Interfacing conducting polymer nanotubes with the central nervous system: chronic neural recording using poly(3,4-ethylenedioxythiophene) nanotubes. *Adv Mater* 2009;21:3764–70.
- [44] Abidian MR, Corey JM, Kipke DR, Martin DC. Conducting-polymer nanotubes improve electrical properties, mechanical adhesion, neural attachment, and neurite outgrowth of neural electrodes. *Small* 2010;6:421–9.
- [45] Huang JX, Virji S, Weiller BH, Kaner RB. Polyaniline nanofibers: facile synthesis and chemical sensors. *J Am Chem Soc* 2003;125:314–5.
- [46] Huang JX, Kaner RB. A general chemical route to polyaniline nanofibers. *J Am Chem Soc* 2004;126:851–5.
- [47] Chiou NR, Epstein AJ. Polyaniline nanofibers prepared by dilute polymerization. *Adv Mater* 2005;17:1679–83.
- [48] Wan MX. A template-free method towards conducting polymer nanostructures. *Adv Mater* 2008;20:2926–32.
- [49] Wan MX, Huang J, Shen YQ. Microtubes of conducting polymers. *Synth Met* 1999;101:708–11.
- [50] Huang JX, Kaner RB. Nanofiber formation in the chemical polymerization of aniline: a mechanistic study. *Angew Chem Int Ed* 2004;43:5817–21.
- [51] Jang J, Yoon H. Facile fabrication of polypyrrole nanotubes using reverse microemulsion polymerization. *Chem Commun* 2003:720–1.
- [52] Liu H, Hu XB, Wang JY, Boughton RI. Structure, conductivity, and thermopower of crystalline polyaniline synthesized by the ultrasonic irradiation polymerization method. *Macromolecules* 2002;35:9414–9.
- [53] Pillalamarri SK, Blum FD, Tokuhito AT, Story JG, Bertino MF. Radiolytic synthesis of polyaniline nanofibers: a new templateless pathway. *Chem Mater* 2005;17:227–9.
- [54] Pillalamarri SK, Blum FD, Tokuhito AT, Bertino MF. One-pot synthesis of polyaniline-metal nanocomposites. *Chem Mater* 2005;17:5941–4.
- [55] Werake LK, Story JG, Bertino MF, Pillalamarri SK, Blum FD. Photolithographic synthesis of polyaniline nanofibers. *Nanotechnology* 2005;16:2833–7.
- [56] Zhang LJ, Long YZ, Chen ZJ, Wan MX. The effect of hydrogen bonding on self-assembled polyaniline nanostructures. *Adv Funct Mater* 2004;14:693–8.
- [57] Ding HJ, Shen JY, Wan MX, Chen ZJ. Formation mechanism of polyaniline nanotubes by a simplified template-free method. *Macromol Chem Phys* 2008;209:864–71.
- [58] Ding HJ, Wan MX, Wei Y. Controlling the diameter of polyaniline nanofibers by adjusting the oxidant redox potential. *Adv Mater* 2007;19:465–9.
- [59] Ding HJ, Long YZ, Shen JY, Wan MX. Fe<sub>2</sub>(SO<sub>4</sub>)<sub>3</sub> as a binary oxidant and dopant to thin polyaniline nanowires with high conductivity. *J Phys Chem B* 2010;114:115–9.
- [60] Yan Y, Deng K, Yu Z, Wei ZX. Tuning the supramolecular chirality of polyaniline by methyl substitution. *Angew Chem Int Edit* 2009;48:2003–6.
- [61] Zhang LJ, Wan MX. Self-assembly of polyaniline—from nanotubes to hollow microspheres. *Adv Funct Mater* 2003;13:815–20.
- [62] Zhang LJ, Wan MX, Wei Y. Hollow polyaniline microspheres with conductive and fluorescent function. *Macromol Rapid Commun* 2006;27:888–93.
- [63] Zhang ZM, Wei ZX, Zhang LJ, Wan MX. Polyaniline nanotubes and their dendrites doped with different naphthalene sulfonic acids. *Acta Mater* 2005;53:1373–9.

- [64] Tang QW, Wu JH, Sun XM, Li QH, Lin JM. Shape and size control of oriented polyaniline microstructure by a self-assembly method. *Langmuir* 2009;25:5253–7.
- [65] Huang ZM, Zhang YZ, Kotaki M, Ramakrishna S. A review on polymer nanofibers by electrospinning and their applications in nanocomposites. *Compos Sci Technol* 2003;63:2223–53.
- [66] Greiner A, Wendorff JH. Functional self-assembled nanofibers by electrospinning. *Adv Polym Sci* 2008;219:107–71.
- [67] Norris ID, Shaker MM, Ko FK, MacDiarmid AG. Electrostatic fabrication of ultrafine conducting fibers: polyaniline/polyethylene oxide blends. *Synth Met* 2000;114:109–14.
- [68] MacDiarmid AG, Jones Jr WE, Norris ID, Gao J, Johnson Jr AT, Pinto NJ, Hone J, Han B, Ko FK, Okuzaki H, Llaguno M. Electrostatically-generated nanofibers of electronic polymers. *Synth Met* 2001;119:27–30.
- [69] Cárdenas JR, de França MGO, de Vasconcelos EA, de Azevedo WM, da Silva Jr EF. Growth of sub-micron fibres of pure polyaniline using the electrospinning technique. *J Phys D: Appl Phys* 2007;40:1068–71.
- [70] Kang TS, Lee SW, Joo J, Lee JY. Electrically conducting polypyrrole fibers spun by electrospinning. *Synth Met* 2005;153:61–4.
- [71] Chronakis IS, Grapenson S, Jakob A. Conductive polypyrrole nanofibers via electrospinning: electrical and morphological properties. *Polymer* 2006;47:1597–603.
- [72] Laforge A, Robitaille L. Fabrication of poly-3-hexylthiophene/polyethylene oxide nanofibers using electrospinning. *Synth Met* 2008;158:577–84.
- [73] Shin MK, Kim YJ, Kim SI, Kim SK, Lee H, Spinks GM, Kim SJ. Enhanced conductivity of aligned PANi/PEO/MWNT nanofibers by electrospinning. *Sensor Actuat B-Chem* 2008;134:122–6.
- [74] Pinto NJ, Johnson Jr AT, Mueller CH, Theofylaktos N, Robinson DC, Miranda FA. Electrospun polyaniline/polyethylene oxide nanofiber field-effect transistor. *Appl Phys Lett* 2003;83:4244–6.
- [75] Liu HQ, Reccius CH, Craighead HG. Single electrospun regioregular poly(3-hexylthiophene) nanofiber field-effect transistor. *Appl Phys Lett* 2005;87, 253106/1–3.
- [76] Liu HQ, Kameoka J, Czaplewski DA, Craighead HG. Polymeric nanowire chemical sensor. *Nano Lett* 2004;4:671–5.
- [77] Zhang FL, Nyberg T, Inganäs O. Conducting polymer nanowires and nanodots made with soft lithography. *Nano Lett* 2002;2:1373–7.
- [78] Hu ZJ, Muls B, Gence L, Serban DA, Hofkens J, Melinte S, Nysten B, Demoustier-Champagne S, Jonas AM. High-throughput fabrication of organic nanowire devices with preferential internal alignment and improved performance. *Nano Lett* 2007;7:3639–44.
- [79] Huang CY, Dong B, Lu N, Yang NJ, Gao LG, Tian L, Qi DP, Wu Q, Chi LF. A strategy for patterning conducting polymers using nanoimprint lithography and isotropic plasma etching. *Small* 2009;5:583–6.
- [80] Niu XZ, Peng SL, Liu LY, Wen WJ, Sheng P. Characterizing and patterning of PDMS-based conducting composites. *Adv Mater* 2007;19:2682–6.
- [81] Ozturk B, Blackledge C, Flanders BN, Grischkowsky DR. Reproducible interconnects assembled from gold nanorods. *Appl Phys Lett* 2006;88, 073108/1–3.
- [82] Yun M, Myung NV, Vasquez RP, Lee C, Menke E, Penner RM. Electrochemically grown wires for individual addressable sensor arrays. *Nano Lett* 2004;4:419–22.
- [83] Ramanathan K, Bangar MA, Yun MH, Chen W, Mulchandani A, Myung NV. Individually addressable conducting polymer nanowires array. *Nano Lett* 2004;4:1237–9.
- [84] Das A, Lei CH, Elliott M, Macdonald JE, Turner ML. Non-lithographic fabrication of PEDOT nano-wires between fixed Au electrodes. *Org Electron* 2006;7:181–7.
- [85] Lee I, Park HI, Park S, Kim MJ, Yun MH. Highly reproducible single polyaniline nanowire using electrophoresis method. *Nano* 2008;3:75–82.
- [86] Thapa PS, Yu DJ, Wickstedt JP, Hadwiger JA, Barisci JN, Baughman RH, Flanders BN. Directional growth of polypyrrole and polythiophene wires. *Appl Phys Lett* 2009;94, 033104/1–3.
- [87] Noy A, Miller AE, Klare JE, Weeks BL, Woods BW, DeYoreo JJ. Fabrication of luminescent nanostructures and polymer nanowires using dip-pen nanolithography. *Nano Lett* 2002;2:109–12.
- [88] Samitsu S, Shimomura T, Ito K, Fujimori M, Heike S, Hashizume T. Conductivity measurements of individual poly(3,4-ethylenedioxythiophene)/poly(styrenesulfonate) nanowires on nanoelectrodes using manipulation with an atomic force microscope. *Appl Phys Lett* 2005;86, 233103/1–3.
- [89] Samitsu S, Takanishi Y, Yamamoto J. Self-assembly and one-dimensional alignment of a conducting polymer nanofiber in a nematic liquid crystal. *Macromolecules* 2009;42:4366–8.
- [90] Yonemura H, Yuno K, Yamamoto Y, Yamada S, Fujiwara Y, Tanimoto Y. Orientation of nanowires consisting poly(3-hexylthiophene) using strong magnetic field. *Synth Met* 2009;159:955–60.
- [91] Parthasarathy RV, Martin CR. Template-synthesized polyaniline microtubules. *Chem Mater* 1994;6:1627–32.
- [92] Spatz JP, Lorenz B, Weishaupt K, Hochheimer HD, Menon V, Parthasarathy R, Martin CR, Bechtold J, Hor PH. Observation of crossover from three- to two-dimensional variable-range hopping in template-synthesized polypyrrole and polyaniline. *Phys Rev B* 1994;50:14888–92.
- [93] Orgzall I, Lorenz B, Ting ST, Hor PH, Menon V, Martin CR, Hochheimer HD. Thermopower and high-pressure electrical conductivity measurements of template synthesized polypyrrole. *Phys Rev B* 1996;54:16654–8.
- [94] Long YZ, Chen ZJ, Wang NL, Zhang ZM, Wan MX. Resistivity study of polyaniline doped with protonic acids. *Physica B* 2003;325:208–13.
- [95] Long YZ, Chen ZJ, Zheng P, Wang NL, Zhang ZM, Wan MX. Low-temperature resistivities of nanotubular polyaniline doped with H<sub>3</sub>PO<sub>4</sub> and  $\beta$ -naphthalene sulfonic acid. *J Appl Phys* 2003;93:2926–65.
- [96] Long YZ, Zhang LJ, Ma YJ, Chen ZJ, Wang NL, Zhang Z, Wan MX. Electrical conductivity of an individual polyaniline nanotube synthesized by a self-assembly method. *Macromol Rapid Commun* 2003;24:938–42.
- [97] Park JG, Lee SH, Kim B, Park YW. Electrical resistivity of polypyrrole nanotube measured by conductive scanning probe microscope: The role of contact force. *Appl Phys Lett* 2002;81:4625–7.
- [98] Park JG, Kim B, Lee SH, Park YW. Current-voltage characteristics of polypyrrole nanotube in both vertical and lateral electrodes configuration. *Thin Solid Films* 2003;438–439:18–22.
- [99] Saha SK, Su YK, Lin CL, Jaw DW. Current-voltage characteristics of conducting polypyrrole nanotubes using atomic force microscopy. *Nanotechnology* 2004;15:66–9.
- [100] Cai CD, Zhou JZ, Qi L, Xi YY, Lan BB, Wu LL, Lin ZH. Conductance of a single conducting polyaniline nanowire. *Acta Phys Chim Sin* 2005;21:343–6.
- [101] Xiong SX, Wang Q, Chen YH. Study on electrical conductivity of single polyaniline microtube. *Mater Lett* 2007;61:2965–8.
- [102] Liu L, Zhao YM, Jia NQ, Zhou Q, Zhao CJ, Yan MM, Jiang ZY. Electrochemical fabrication and electronic behavior of polypyrrole nano-fiber array devices. *Thin Solid Films* 2006;503:241–5.
- [103] Kim GT, Burghard M, Suh DS, Liu K, Park JG, Roth S, Park YW. Conductivity and magnetoresistance of polyacetylene fiber network. *Synth Met* 1999;105:207–10.
- [104] Park JH, Yu HY, Park JG, Kim B, Lee SH, Olofsson L, Persson SHM, Park YW. Non-linear I-V characteristics of MEH-PPV patterned on sub-micrometer electrodes. *Thin Solid Films* 2001;393:129–31.
- [105] Park JG, Kim GT, Krstic V, Kim B, Lee SH, Roth S, Burghard M, Park YW. Nanotransport in polyacetylene single fiber: toward the intrinsic properties. *Synth Met* 2001;119:53–6.
- [106] Lee HJ, Jin ZX, Aleshin AN, Lee JY, Goh MJ, Akagi K, Kim YS, Kim DW, Park YW. Dispersion and current-voltage characteristics of helical polyacetylene single fibers. *J Am Chem Soc* 2004;126:16722–3.
- [107] Aleshin AN, Lee HJ, Park YW, Akagi K. One-dimensional transport in polymer nanofibers. *Phys Rev Lett* 2004;93:196601.
- [108] Aleshin AN, Lee HJ, Jhang SH, Kim HS, Akagi K, Park YW. Coulomb-blockade transport in quasi-one-dimensional polymer nanofibers. *Phys Rev B* 2005;72, 153202/1–4.
- [109] Long YZ, Chen ZJ, Wang NL, Ma YJ, Zhang Z, Zhang LJ, Wan MX. Electrical conductivity of a single conducting polyaniline nanotube. *Appl Phys Lett* 2003;83:1863–5.
- [110] Long YZ, Zhang LJ, Chen Z, Huang K, Yang YS, Xiao HM, Wan MX, Jin AZ, Gu CZ. Electronic transport in single polyaniline and polypyrrole microtubes. *Phys Rev B* 2005;71, 165412/1–7.
- [111] Duvail JL, Long YZ, Cuenot S, Chen ZJ, Gu CZ. Tuning electrical properties of conjugated polymer nanowires with the diameter. *Appl Phys Lett* 2007;90, 102114/1–3.
- [112] Zhang XY, Lee JS, Lee GS, Cha DK, Kim MJ, Yang DJ, Manohar SK. Chemical synthesis of PEDOT nanotubes. *Macromolecules* 2006;39:470–2.
- [113] Lu GW, Li C, Shen JY, Chen ZJ, Shi GQ. Preparation of highly conductive gold-poly(3,4-ethylenedioxythiophene) nanocables and their conversion to poly(3,4-ethylenedioxy-thiophene) nanotubes. *J Phys Chem C* 2007;111:5926–31.
- [114] Huang K, Zhang YJ, Long YZ, Yuan JH, Han DX, Wang ZJ, Niu L, Chen ZJ. Preparation of highly conductive, self-assembled gold/polyaniline nano-cables and polyaniline nanotubes. *Chem-Eur J* 2006;12:5314–9.

- [115] Long YZ, Xiao HM, Chen ZJ, Wan MX, Jin AZ, Gu CZ. Electrical conductivity of individual polypyrrole microtube. *Chin Phys* 2004;13:1918–21.
- [116] Long YZ, Yin ZH, Li MM, Gu CZ, Duvail JL, Jin AZ, Wan MX. Current-voltage characteristics of individual conducting polymer nanotubes and nanowires. *Chin Phys B* 2009;18:2514–22.
- [117] De Marzi G, Iacopino B, Quinn AJ, Redmond G. Probing intrinsic transport properties of single metal nanowires: direct-write contact formation using a focused ion beam. *J Appl Phys* 2004;96:3458–62.
- [118] Cai ZH, Martin CR. Electronically conductive polymer fibers with mesoscopic diameters show enhanced electronic conductivities. *J Am Chem Soc* 1989;111:4138–9.
- [119] Yoon CO, Reghu M, Moses D, Heeger AJ. Transport near the metal-insulator transition: polypyrrole doped with  $\text{PF}_6$ . *Phys Rev B* 1994;49:10851–63.
- [120] Long YZ, Duvail JL, Chen ZJ, Jin AZ, Gu CZ. Electrical conductivity and current-voltage characteristics of individual conducting polymer PEDOT nanowires. *Chin Phys Lett* 2008;25:3474–7.
- [121] Kaiser AB, Iorns TM, Park JG, Kim B, Lee SH, Park YW. Variation with temperature of the I-V characteristics of polyacetylene nanofibers. *Curr Appl Phys* 2002;2:285–8.
- [122] Kaiser AB, Rogers SA, Park YW. Charge transport in conducting polymers: polyacetylene nanofibers. *Mol Cryst Liq Cryst* 2004;415:115–24.
- [123] Kaiser AB, Park JG, Kim B, Lee SH, Park YW. Polypyrrole microline: current-voltage characteristics and comparison with other conducting polymers. *Curr Appl Phys* 2004;4:497–500.
- [124] Kaiser AB, Park YW. Comparison of tunnelling conduction in polyacetylene nanofibers, CDW and SDW systems. *Synth Met* 2003;135:245–7.
- [125] Kaiser AB, Park YW. Current-voltage characteristics of conducting polymers and carbon nanotubes. *Synth Met* 2005;152:181–4.
- [126] Saha SK. Room-temperature single-electron tunneling in conducting polypyrrole nanotube. *Appl Phys Lett* 2002;81:3645–7.
- [127] Rahman A, Sanyal MK. Observation of charge density wave characteristics in conducting polymer nanowires: Possibility of Wigner crystallization. *Phys Rev B* 2007;76, 045110/1–6.
- [128] Kang N, Hu JS, Kong WJ, Lu L, Zhang DL, Pan ZW, Xie SS. Consistent picture of strong electron correlation from magnetoresistance and tunneling conductance measurements in multiwall carbon nanotubes. *Phys Rev B* 2002;66, 241403/1–4.
- [129] Long YZ, Wang WL, Bai FL, Chen ZJ, Jin AZ, Gu CZ. Current-voltage characteristics of an individual helical CdS nanowire rope. *Chin Phys B* 2008;17:1389–93.
- [130] Long YZ, Yin ZH, Chen ZJ, Jin AZ, Gu CZ, Zhang HT, Chen XH. Low-temperature electronic transport in single  $\text{K}_{0.27}\text{MnO}_2 \cdot 0.5\text{H}_2\text{O}$  nanowires: enhanced electron-electron interaction. *Nanotechnology* 2008;19, 215708/1–5.
- [131] Ma YJ, Zhou F, Lu L, Zhang Z. Low-temperature transport properties of individual  $\text{SnO}_2$  nanowires. *Solid State Commun* 2004;130:313–6.
- [132] Ma YJ, Zhang Z, Zhou F, Lu L, Jin AZ, Gu CZ. Hopping conduction in single ZnO nanowires. *Nanotechnology* 2005;16:746–9.
- [133] Yuen JD, Menon R, Coates NE, Namdas EB, Cho S, Hannahs ST, Moses D, Heeger AJ. Nonlinear transport in semiconducting polymers at high carrier densities. *Nat Mater* 2009;8:572–5.
- [134] Yin ZH, Long YZ, Gu CZ, Wan MX, Duvail JL. Current-voltage characteristics in individual polypyrrole nanotube, poly(3,4-ethylene-dioxy-thiophene) nanowire, polyaniline nanotube, and CdS nanorope. *Nanoscale Res Lett* 2009;4:63–9.
- [135] Long YZ, Duvail JL, Li MM, Gu CZ, Liu Z, Ringer SP. Electrical conductivity studies on individual conjugated polymer nanowires: two-probe and four-probe results. *Nanoscale Res Lett* 2010;5:237–42.
- [136] Lin YH, Chiu SP, Lin JJ. Thermal fluctuation-induced tunneling conduction through metal nanowire contacts. *Nanotechnology* 2008;19, 365201/1–7.
- [137] Lan C, Srisungsithisunti P, Amama PB, Fisher TS, Xu XF, Reifenger RG. Measurement of metal/carbon nanotube contact resistance by adjusting contact length using laser ablation. *Nanotechnology* 2008;19, 125703/1–7.
- [138] Stern E, Cheng G, Klemic JF, Broomfield E, Turner-Evans D, Li C, Zhou C, Reed MA. Methods for fabricating Ohmic contacts to nanowires and nanotubes. *J Vac Sci Technol B* 2006;24:231–6.
- [139] Lin YF, Jian WB. The impact of nanocontact on nanowire based nanoelectronics. *Nano Lett* 2008;8:3146–50.
- [140] Long YZ, Duvail JL, Wang QT, Li MM, Gu CZ. Electronic transport through crossed conducting polymer nanowires. *J Mater Res* 2009;24:3018–22.
- [141] Kozub VI, Aleshin AN, Suh DS, Park YW. Evidence of magnetoresistance for nanojunction-controlled transport in heavily doped polyacetylene. *Phys Rev B* 2002;65, 224204/1–5.
- [142] Long YZ, Chen ZJ, Shen JY, Zhang ZM, Zhang LJ, Huang K, Wan MX, Jin AZ, Gu CZ, Duvail JL. Magnetoresistance studies of polymer nanotube/wire pellets and single polymer nanotubes/wires. *Nanotechnology* 2006;17:5903–11.
- [143] (a) Long YZ, Huang K, Yuan JH, Han DX, Niu L, Chen ZJ, Gu CZ, Jin AZ, Duvail JL. Electrical conductivity of a single Au/polyaniline microfiber. *Appl Phys Lett* 2006;88, 162113/1–3; (b) Long YZ, Duvail JL, Chen ZJ, Jin AZ, Gu CZ. Electrical properties of isolated poly(3,4-ethylenedioxythiophene) nanowires prepared by template synthesis. *Polym Adv Technol* 2009;20:541–4.
- [144] Bozdag KD, Chiou NR, Prigodin VN, Epstein AJ. Magnetic field, temperature and electric field dependence of magneto-transport for polyaniline nanofiber networks. *Synth Met* 2010;160:271–4.
- [145] (a) Park YW. Magneto resistance of polyacetylene nanofibers. *Chem Soc Rev* 2010;39:2428–38; (b) Choi A, Lee HJ, Kaiser AB, Jhang SH, Lee SH, Yoo JS, Kim HS, Nam YW, Park SJ, Yoo HN, Aleshin AN, Goh M, Akagi K, Kaner RB, Brooks JS, Svensson J, Brazovskii SA, Kirova NN, Park YW. Suppression of the magneto resistance in high electric fields of polyacetylene nanofibers. *Synth Met* 2010;160:1349–53.
- [146] Shklovskii BI, Efros AL. *Electronic properties of doped semiconductors*. Berlin: Springer; 1984.
- [147] Weinberger BR, Kaufner J, Heeger AJ, Pron A, MacDiarmid AG. Magnetic susceptibility of doped polyacetylene. *Phys Rev B* 1979;20:223–30.
- [148] Ginder JM, Richter AF, MacDiarmid AG, Epstein AJ. Insulator-to-metal transition in polyaniline. *Solid State Commun* 1987;63:97–101.
- [149] Raghunathan A, Natarajan TS, Rangarajan G, Dhawan SK, Trivedi DC. Charge transport and optical and magnetic properties of polyaniline synthesized with use of organic acids. *Phys Rev B* 1993;47:13189–96.
- [150] Kahol PK, Raghunathan A, McCormick BJ. A magnetic susceptibility study of emeraldine base polyaniline. *Synth Met* 2004;140:261–7.
- [151] Kahol PK, Ho JC, Chen YY, Wang CR, Neeleshwar S, Tsai CB, Wessling B. Heat capacity, electron paramagnetic resonance, and dc conductivity investigations of dispersed polyaniline and poly(ethylene dioxythiophene). *Synth Met* 2005;153:169–72.
- [152] Kahol PK, Ho JC, Chen YY, Wang CR, Neeleshwar S, Tsai CB, Wessling B. On metallic characteristics in some conducting polymers. *Synth Met* 2005;151:65–72.
- [153] Long YZ, Chen ZJ, Shen JY, Zhang ZM, Zhang LJ, Xiao HM, Wan MX, Duvail JL. Magnetic properties of conducting polymer nanostructures. *J Phys Chem B* 2006;110:23228–33.
- [154] Djurado D, Pron A, Travers JP, Duque JGS, Pagliuso PG, Rettori C, Chianaglia DL, Walmsley L. Magnetic field dependent magnetization of a conducting plasticized poly(aniline) film. *J Phys: Condens Matter* 2008;20, 285228/1–7.
- [155] Beau B, Travers JP, Banka E. NMR evidence for heterogeneous disorder and quasi-1D metallic state in polyaniline CSA. *Synth Met* 1999;101:772–5.
- [156] Nalwa HS. Phase transitions in polypyrrole and polythiophene conducting polymers demonstrated by magnetic susceptibility measurements. *Phys Rev B* 1989;39:5964–74.
- [157] Shimoi Y, Abe S. Theory of triplet exciton polarons and photoinduced absorption in conjugated polymers. *Phys Rev B* 1994;49:14113–21.
- [158] Nascimento OR, de Oliveira AJA, Pereira EC, Correa AA, Walmsley L. The ferromagnetic behaviour of conducting polymers revisited. *J Phys: Condens Matter* 2008;20, 035214/1–8.
- [159] Varela-Álvarez A, Sordo JA. A suitable model for emeraldine salt. *J Chem Phys* 2008;128, 174706/1–7.
- [160] Moses D, Denenstein A, Pron A, Heeger AJ, MacDiarmid AG. Specific heats of pure and doped polyacetylene. *Solid State Commun* 1980;36:219–24.
- [161] Skákalová V, Fedorko P. Thermal properties of powder polyacetylene. *Synth Met* 1993;55–57:135–40.
- [162] Raghunathan A, Kahol PK, Ho JC, Chen YY, Yao YD, Lin YS, Wessling B. Low-temperature heat capacities of polyaniline and polyaniline polymethylmethacrylate blends. *Phys Rev B* 1998;58:15955–8.

- [163] Gilani TH. Evidence for metal-like electronic contribution in low-temperature heat capacity of polypyrrole. *J Phys Chem B* 2005;109:19204–7.
- [164] Xu J, Luo JL, Chen ZJ, Long YZ, Bai HY, Wan MX, Wang NL. The specific heat of polyaniline at low-temperature. *Acta Phys Sin* 2003;52:947–51.
- [165] Long YZ, Luo JL, Xu J, Chen ZJ, Zhang LJ, Li JC, Wan MX. Specific heat and magnetic susceptibility of polyaniline nanotubes: inhomogeneous disorder. *J Phys: Condens Matter* 2004;16:1123–30.
- [166] Carini G, D'Angelo G, Tripodo G, Bartolotta A, Di Marco G. Low-temperature excess specific heat and fragility in semicrystalline polymers. *Phys Rev B* 1996;54:15056–63.
- [167] Avogadro A, Aldrovandi S, Borsa F, Carini G. Specific-heat study of low-energy excitations in glasses. *Phil Mag B* 1987;56:227–36.
- [168] Joo J, Long SM, Pouget JP, Oh EJ, MacDiarmid AG, Epstein AJ. Charge transport of the mesoscopic metallic state in partially crystalline polyanilines. *Phys Rev B* 1998;57:9567–80.
- [169] Cho SI, Kwon WJ, Choi SJ, Kim P, Park SA, Kim J, Son SJ, Xiao R, Kim SH, Lee SB. Nanotube-based ultrafast electrochromic display. *Adv Mater* 2005;17:171–5.
- [170] Kim BK, Kim YH, Won K, Chang H, Choi Y, Kong KJ, Rhyu BW, Kim JJ, Lee JO. Electrical properties of polyaniline nanofiber synthesized with biocatalyst. *Nanotechnology* 2005;16:1177–81.
- [171] Cho SI, Lee SB. Fast electrochemistry of conductive polymer nanotubes: Synthesis, mechanism, and application. *Acc Chem Res* 2008;41:699–707.
- [172] Duvail JL, Long Y, Rétho P, Louarn G, Dauginet De Pra L, Demoustier-Champagne S. Enhanced electroactivity and electrochromism in PEDOT nanowires. *Mol Cryst Liq Cryst* 2008;485:835–42.
- [173] Wang XH, Shao MW, Shao G, Fu Y, Wang SW. Reversible and efficient photocurrent switching of ultra-long polypyrrole nanowires. *Synth Met* 2009;159:273–6.
- [174] Wang XH, Shao MW, Shao G, Wu ZC, Wang SW. A facile route to ultra-long polyaniline nanowires and the fabrication of photo-switch. *J Colloid Interface Sci* 2009;332:74–7.
- [175] Huang JX, Kaner RB. Flash welding of conducting polymer nanofibers. *Nat Mater* 2004;3:783–6.
- [176] Li D, Xia YN. Nanomaterials: Welding and patterning in a flash. *Nat Mater* 2004;3:753–4.
- [177] Baker CO, Shedd B, Innis PC, Whitten PG, Spinks GM, Wallace GG, Kaner RB. Monolithic actuators from flash-welded polyaniline nanofibers. *Adv Mater* 2008;20:155–8.
- [178] Huang K, Wan MX. Self-assembled polyaniline nanostructures with photoisomerization function. *Chem Mater* 2002;14:3486–92.
- [179] Tan EPS, Lim CT. Mechanical characterization of nanofibers—a review. *Compos Sci Technol* 2006;66:1102–11.
- [180] Cuenot S, Demoustier-Champagne S, Nysten B. Elastic modulus of polypyrrole nanotubes. *Phys Rev Lett* 2000;85:1690–3.
- [181] Cuenot S, Frétygny C, Demoustier-Champagne S, Nysten B. Measurement of elastic modulus of nanotubes by resonant contact atomic force microscopy. *J Appl Phys* 2003;93:5650–5.
- [182] Cuenot S, Frétygny C, Demoustier-Champagne S, Nysten B. Surface tension effect on the mechanical properties of nanomaterials measured by atomic force microscopy. *Phys Rev B* 2004;69:165410/1–5.
- [183] (a) Lee SW, Kim B, Lee DS, Lee HJ, Park JG, Ahn SJ, Campbell EEB, Park YW. Fabrication and mechanical properties of suspended one-dimensional polymer nanostructures: polypyrrole nanotube and helical polyacetylene nanofiber. *Nanotechnology* 2006;17:992–6; (b) Foroughi J, Ghorbani SR, Peleckis G, Spinks GM, Wallace GG, Wang XL, Dou SX. The mechanical and the electrical properties of conducting polypyrrole fibers. *J Appl Phys* 2010;107:103712/1–4.
- [184] Sun L, Han RPS, Wang J, Lim CT. Modeling the size-dependent elastic properties of polymeric nanofibers. *Nanotechnology* 2008;19:455706/1–8.
- [185] Arinstein A, Burman M, Gendelman O, Zussman E. Effect of supramolecular structure on polymer nanofiber elasticity. *Nat Nanotechnol* 2007;2:59–62.
- [186] Burman M, Arinstein A, Zussman E. Free flight of an oscillated string pendulum as a tool for the mechanical characterization of an individual polymer nanofiber. *Appl Phys Lett* 2008;93:193118/1–3.
- [187] Muraoka M, Tobe R. Mechanical characterization of nanowires based on optical diffraction images of the bent shape. *J Nanosci Nanotechnol* 2009;9:4566–74.
- [188] Gordon MJ, Baron T, Dhalluin F, Gentile P, Ferret P. Size effects in mechanical deformation and fracture of cantilevered silicon nanowires. *Nano Lett* 2009;9:525–9.
- [189] Guo JG, Zhao YP. The size-dependent bending elastic properties of nanobeams with surface effects. *Nanotechnology* 2007;18:295701/1–6.
- [190] Olmedo L, Hourquebie P, Jousse F. Microwave absorbing materials based on conducting polymers. *Adv Mater* 1993;5:373–7.
- [191] Chandrasekhar P, Naishadham K. Broadband microwave absorption and shielding properties of a poly(aniline). *Synth Met* 1999;105:115–20.
- [192] Joo J, Lee CY. High frequency electromagnetic interference shielding response of mixtures and multilayer films based on conducting polymers. *J Appl Phys* 2000;88:513–8.
- [193] Wan MX, Li JC, Li SZ. Microtubules of polyaniline as new microwave absorbent materials. *Polym Adv Technol* 2001;12:651–7.
- [194] Liu CY, Jiao YC, Zhang LX, Xue MB, Zhang FS. Electromagnetic wave absorbing property of polyaniline/polystyrene composites. *Acta Metall Sinica* 2007;43:409–12.
- [195] Jang J, Chang M, Yoon H. Chemical sensors based on highly conductive poly(3,4-ethylenedioxythiophene) nanorods. *Adv Mater* 2005;17:1616–20.
- [196] Virji S, Huang JX, Kaner RB, Weiller BH. Polyaniline nanofiber gas sensors: examination of response mechanisms. *Nano Lett* 2004;4:491–6.
- [197] Sutar DS, Padma N, Aswal DK, Deshpande SK, Gupta SK, Yakhmi JV. Preparation of nanofibrous polyaniline films and their application as ammonia gas sensor. *Sens Actuat B-Chem* 2007;128:286–92.
- [198] Li ZF, Blum FD, Bertino MF, Kim CS, Pillalamarri SK. One-step fabrication of a polyaniline nanofiber vapor sensor. *Sens Actuat B-Chem* 2008;134:31–5.
- [199] Yoon H, Chang M, Jang J. Formation of 1D poly(3,4-ethylenedioxythiophene) nanomaterials in reverse micromulsions and their application to chemical sensors. *Adv Funct Mater* 2007;17:431–6.
- [200] Chen YX, Luo Y. Precisely defined heterogeneous conducting polymer nanowire arrays – Fabrication and chemical sensing applications. *Adv Mater* 2009;21:2040–4.
- [201] Rajesh, Ahuja T, Kumar D. Recent progress in the development of nano-structured conducting polymers/nanocomposites for sensor applications. *Sens Actuat B-Chem* 2009;136:275–86.
- [202] Antohe VA, Radu A, Mátéfi-Tempfli M, Attout A, Yunus S, Bertrand P, Dutu CA, Vlad A, Melinte S, Mátéfi-Tempfli S, Piraux L. Nanowire-templated microelectrodes for high-sensitivity pH detection. *Appl Phys Lett* 2009;94:073118/1–3.
- [203] Shirsat MD, Bangar MA, Deshusses MA, Myung NV, Mulchandani A. Polyaniline nanowires-gold nanoparticles hybrid network based chemiresistive hydrogen sulfide sensor. *Appl Phys Lett* 2009;94:083502/1–3.
- [204] Bai H, Zhao L, Lu CH, Li C, Shi GQ. Composite nanofibers of conducting polymers and hydrophobic insulating polymers: preparation and sensing applications. *Polymer* 2009;50:3292–301.
- [205] Yu XF, Li YX, Kalantar-zadeh K. Synthesis and electrochemical properties of template-based polyaniline nanowires and template-free nanofibrillar arrays: Two potential nanostructures for gas sensors. *Sens Actuat B-Chem* 2009;136:1–7.
- [206] Bai H, Shi GQ. Gas sensors based on conducting polymers. *Sensors* 2007;7:267–307.
- [207] Lu HH, Lin CY, Hsiao TC, Fang YY, Ho KC, Yang DF, Lee CK, Hsu SM, Lin CW. Electrical properties of single and multiple poly(3,4-ethylenedioxythiophene) nanowires for sensing nitric oxide gas. *Anal Chim Acta* 2009;640:68–74.
- [208] Wang YJ, Coti KK, Wang J, Alam MM, Shyue JJ, Lu WX, Padture NP, Tseng HR. Individually addressable crystalline conducting polymer nanowires in a microelectrode sensor array. *Nanotechnology* 2007;18:424021/1–7.
- [209] Dan YP, Cao YY, Mallouk TE, Evoy S, Johnson ATC. Gas sensing properties of single conducting polymer nanowires and the effect of temperature. *Nanotechnology* 2009;20:434014/1–4.
- [210] Cao Y, Kovalev AE, Xiao R, Kim J, Mayer TS, Mallouk TE. Electrical transport and chemical sensing properties of individual conducting polymer nanowires. *Nano Lett* 2008;8:4653–8.
- [211] Pringsheim E, Zimin D, Wolfbeis OS. Fluorescent beads coated with polyaniline: A novel nanomaterial for sensing of pH. *Adv Mater* 2001;13:819–22.
- [212] Gu FX, Zhang L, Yin XF, Tong LM. Polymer single-nanowire optical sensors. *Nano Lett* 2008;8:2757–61.
- [213] Gu FX, Yin XF, Yu HK, Wang P, Tong LM. Polyaniline/polystyrene single-nanowire devices for highly selective optical detection of gas mixtures. *Opt Express* 2009;17:11230–5.

- [214] Gao M, Dai L, Wallace GG. Biosensors based on aligned carbon nanotubes coated with inherently conducting polymers. *Electroanalysis* 2003;15:1089–94.
- [215] Zhang LJ, Peng H, Kilmartin PA, Soeller C, Travas-Sejdic J. Polymeric acid doped polyaniline nanotubes for oligonucleotide sensors. *Electroanalysis* 2007;19:870–5.
- [216] Peng H, Zhang LJ, Spires J, Soeller C, Travas-Sejdic J. Synthesis of a functionalized polythiophene as an active substrate for a label-free electrochemical genosensor. *Polymer* 2007;48:3413–9.
- [217] Langer JJ, Langer K, Barczyński P, Warchoł J, Bartkowiak KH. New “ON-OFF”-type nanobiosensor. *Biosens Bioelectron* 2009;24:2947–9.
- [218] Horng YY, Hsu YK, Ganguly A, Chen CC, Chen LC, Chen KH. Direct-growth of polyaniline nanowires for enzyme-immobilization and glucose detection. *Electrochem Commun* 2009;11:850–3.
- [219] Xie H, Luo SC, Yu HH. Electric-field-assisted growth of functionalized poly(3,4-ethylenedioxythiophene) nanowires for label-free protein detection. *Small* 2009;5:2611–7.
- [220] Huang J, Wei ZX, Chen JC. Molecular imprinted polypyrrole nanowires for chiral amino acid recognition. *Sens Actuat B-Chem* 2008;134:573–8.
- [221] Yang JY, Martin DC. Microporous conducting polymers on neural microelectrode arrays: 1 Electrochemical deposition. *Sens Actuat B-Chem* 2004;101:133–42.
- [222] Herland A, Inganäs O. Conjugated polymers as optical probes for protein interactions and protein conformations. *Macromol Rapid Commun* 2007;28:1703–13.
- [223] Xia L, Wei ZX, Wan MX. Conducting polymer nanostructures and their application in biosensors. *J Colloid Interface Sci* 2010;341:1–11.
- [224] Zhu Y, Feng L, Xia F, Zhai J, Wan MX, Jiang L. Chemical dual-responsive wettability of superhydrophobic PANI-PAN coaxial nanofibers. *Macromol Rapid Commun* 2007;28:1135–41.
- [225] Zhu Y, Li JM, Wan MX, Jiang L. Reversible wettability switching of polyaniline-coated fabric, triggered by ammonia gas. *Macromol Rapid Commun* 2007;28:2230–6.
- [226] Qi PF, Javey A, Rolandi M, Wang Q, Yenilmez E, Dai HJ. Miniature organic transistors with carbon nanotubes as quasi-one-dimensional electrodes. *J Am Chem Soc* 2004;126:11774–5.
- [227] Alam MM, Wang J, Guo YY, Lee SP, Tseng HR. Electrolyte-gated transistors based on conducting polymer nanowire junction arrays. *J Phys Chem B* 2005;109:12777–84.
- [228] Lee SY, Choi GR, Lim H, Lee KM, Lee SK. Electronic transport characteristics of electrolyte-gated conducting polyaniline nanowire field-effect transistors. *Appl Phys Lett* 2009;95:013113/1–3.
- [229] Park S, Chung SW, Mirkin CA. Hybrid organic–inorganic, rod-shaped nanoresistors and diodes. *J Am Chem Soc* 2004;126:11772–3.
- [230] Pinto NJ, González R, Johnson Jr AT, MacDiarmid AG. Electrospun hybrid organic/inorganic semiconductor Schottky nanodiode. *Appl Phys Lett* 2006;89:033505/1–3.
- [231] Pérez R, Pinto NJ, Johnson Jr AT. Influence of temperature on charge transport and device parameters in an electrospun hybrid organic/inorganic semiconductor Schottky diode. *Synth Met* 2007;157:231–4.
- [232] Granström M, Berggren M, Inganäs O. Micrometer- and nanometer-sized polymeric light-emitting diodes. *Science* 1995;267:1479–81.
- [233] Granström M, Berggren M, Inganäs O. Polymeric light-emitting diodes of submicron size – Structures and developments. *Synth Met* 1996;76:141–3.
- [234] Boroumand FA, Fry PW, Lidzey DG. Nanoscale conjugated-polymer light-emitting diodes. *Nano Lett* 2005;5:67–71.
- [235] Grimsdale AC, Chan KL, Martin RE, Jokisz PG, Holmes AB. Synthesis of light-emitting conjugated polymers for applications in electroluminescent devices. *Chem Rev* 2009;109:897–1091.
- [236] Wang CW, Wang Z, Li MK, Li HL. Well-aligned polyaniline nanofibril array membrane and its field emission property. *Chem Phys Lett* 2001;341:431–4.
- [237] Kim BH, Kim MS, Park KT, Lee JK, Park DH, Joo J, Yu SG, Lee SH. Characteristics and field emission of conducting poly(3,4-ethylenedioxythiophene) nanowires. *Appl Phys Lett* 2003;83:539–41.
- [238] Yan HL, Zhang L, Shen JY, Chen ZJ, Shi GQ, Zhang BL. Synthesis, property and field-emission behavior of amorphous polypyrrole nanowires. *Nanotechnology* 2006;17:3446–50.
- [239] Cho SI, Choi DH, Kim SH, Lee SB. Electrochemical synthesis and fast electrochromics of poly(3,4-ethylenedioxythiophene) nanotubes in flexible substrate. *Chem Mater* 2005;17:4564–6.
- [240] Cho SI, Xiao R, Lee SB. Electrochemical synthesis of poly(3,4-ethylenedioxythiophene) nanotubes towards fast window-type electrochromic devices. *Nanotechnology* 2007;18:405705/1–5.
- [241] Kim Y, Baek J, Kim MH, Choi HJ, Kim E. Electrochromic nanostructures grown on a silicon nanowire template. *Ultramicroscopy* 2008;108:1224–7.
- [242] Cao Y, Mallouk TE. Morphology of template-grown polyaniline nanowires and its effect on the electrochemical capacitance of nanowire arrays. *Chem Mater* 2008;20:5260–5.
- [243] Bian CQ, Yu AH, Wu HQ. Fibriform polyaniline/nano-TiO<sub>2</sub> composite as an electrode material for aqueous redox supercapacitors. *Electrochem Commun* 2009;11:266–9.
- [244] Zhang XY, Manohar SK. Polyaniline nanofibers: chemical synthesis using surfactants. *Chem Commun* 2004:2360–1.
- [245] Kuila BK, Nandan B, Böhme M, Janke A, Stamm M. Vertically oriented arrays of polyaniline nanorods and their super electrochemical properties. *Chem Commun* 2009:5749–51.
- [246] Wang K, Huang JY, Wei ZX. Conducting polyaniline nanowire arrays for high performance supercapacitors. *J Phys Chem C* 2010;114:8062–7.
- [247] Liu R, Cho SI, Lee SB. Poly(3,4-ethylenedioxythiophene) nanotubes as electrode materials for high-powered supercapacitor. *Nanotechnology* 2008;19:215710/1–8.
- [248] Kim J, Kim SI, Yoo KH. Polypyrrole nanowire-based enzymatic biofuel cells. *Biosens Bioelectron* 2009;25:350–5.
- [249] Brabec CJ, Sariciftci NS, Hummelen JC. Plastic solar cells. *Adv Funct Mater* 2001;11:15–26.
- [250] Shi W, Cao HH, Shen YQ, Song CF, Li DH, Zhang Y, Ge DT. Chemically modified PPyCOOH microtubes as an affinity matrix for protein purification. *Macromol Chem Phys* 2009;210:1379–86.
- [251] Abidian MR, Martin DC. Multifunctional Nanobiomaterials for Neural Interfaces. *Adv Funct Mater* 2009;19:573–85.
- [252] Jager EWH, Smela E, Inganäs O. Microfabricating conjugated polymer actuators. *Science* 2000;290:1540–5.
- [253] Okamoto T, Kato Y, Tada K, Onoda M. Actuator based on doping/undoping-induced volume change in anisotropic polypyrrole film. *Thin Solid Films* 2001;393:383–7.
- [254] Otero TF, Cortes MT. Artificial muscle: movement and position control. *Chem Commun* 2004:284–5.
- [255] Lu W, Smela E, Adams P, Zuccarello G, Mattes BR. Development of solid-in-hollow electrochemical linear actuators using highly conductive polyaniline. *Chem Mater* 2004;16:1615–21.
- [256] He XM, Li C, Chen FE, Shi GQ. Polypyrrole microtubule actuators for seizing and transferring microparticles. *Adv Funct Mater* 2007;17:2911–7.
- [257] Lee AS, Peteu SF, Ly JV, Requicha AAG, Thompson ME, Zhou CW. Actuation of polypyrrole nanowires. *Nanotechnology* 2008;19:165501/1–8.
- [258] Singh PR, Mahajan S, Rajwade S, Contractor AQ. EC-AFM investigation of reversible volume changes with electrode potential in polyaniline. *J Electroanal Chem* 2009;625:16–26.
- [259] Yang XG, Li B, Wang HZ, Hou BR. Anticorrosion performance of polyaniline nanostructures on mild steel. *Prog Org Coat* 2010;69:267–71.
- [260] Saini P, Choudhary V, Singh BP, Mathur RB, Dhawan SK. Polyaniline-MWCNT nanocomposites for microwave absorption and EMI shielding. *Mater Chem Phys* 2009;113:919–26.
- [261] Wang CC, Song JF, Bao HM, Shen QD, Yang CZ. Enhancement of electrical properties of ferroelectric polymers by polyaniline nanofibers with controllable conductivities. *Adv Funct Mater* 2008;18:1299–306.
- [262] Tseng RJ, Huang J, Ouyang J, Kaner RB, Yang Y. Polyaniline nanofiber/gold nanoparticle non-volatile memory. *Nano Lett* 2005;5:1077–80.
- [263] Inganäs O. Hybrid electronics and electrochemistry with conjugated polymers. *Chem Soc Rev* 2010;39:2633–42.
- [264] Park DH, Kim MS, Joo J. Hybrid nanostructures using  $\pi$ -conjugated polymers and nanoscale metals: synthesis, characteristics, and optoelectronic applications. *Chem Soc Rev* 2010;39:2439–52.
- [265] Al-Mashat L, Shin K, Kalantar-Zadeh K, Plessis JD, Han SH, Kojima RW, Kaner RB, Li D, Gou XL, Ippolito SJ, Wlodarski W. Graphene/polyaniline nanocomposite for hydrogen sensing. *J Phys Chem C* 2010;114:16168–73.
- [266] Wu Q, Xu YX, Yao ZY, Liu AR, Shi GQ. Supercapacitors based on flexible graphene/polyaniline nanofiber composite films. *ACS Nano* 2010;4:1963–70.

- [267] Xu JJ, Wang K, Zu SZ, Han BH, Wei ZX. Hierarchical nanocomposites of polyaniline nanowire arrays on graphene oxide sheets with synergistic effect for energy storage. *ACS Nano* 2010;4:5019–26.
- [268] Liu MJ, Liu XL, Wang JX, Wei ZX, Jiang L. Electromagnetic synergistic actuators based on polypyrrole/Fe<sub>3</sub>O<sub>4</sub> hybrid nanotube arrays. *Nano Res* 2010;3:670–5.
- [269] Spitalsky Z, Tasis D, Papagelis K, Galiotis C. Carbon nanotube–polymer composites: Chemistry, processing, mechanical and electrical properties. *Prog Polym Sci* 2010;35:357–401.
- [270] Kuilla T, Bhadra S, Yao DH, Kim NH, Bose S, Lee JH. Recent advances in graphene based polymer composites. *Prog Polym Sci* 2010;35:1350–75.